

Enhanced hyperfine-induced spin dephasing in a magnetic-field gradient

Félix Beaudoin and W. A. Coish

Department of Physics, McGill University, Montréal, Québec, Canada H3A 2T8

(Dated: November 28, 2018)

Magnetic-field gradients are important for single-site addressability and electric-dipole spin resonance of spin qubits in semiconductor devices. We show that these advantages are offset by a potential reduction in coherence time due to the non-uniformity of the magnetic field experienced by a nuclear-spin bath interacting with the spin qubit. We theoretically study spins confined to quantum dots or at single donor impurities, considering both free-induction and spin-echo decay. For quantum dots in GaAs, we find that, in a realistic setting, a magnetic-field gradient can reduce the Hahn-echo coherence time by almost an order of magnitude. This problem can, however, be resolved by applying a moderate external magnetic field to enter a motional averaging regime. For quantum dots in silicon, we predict a cross-over from non-Markovian to Markovian behavior that is unique to these devices. Finally, for very small systems such as single phosphorus donors in silicon, we predict a breakdown of the common Gaussian approximation due to finite-size effects.

PACS numbers: 03.65.Yz, 76.60.Lz, 75.75.-c

I. INTRODUCTION

One of the most intriguing features of spins in semiconductor nanostructures is our ability to systematically determine decoherence mechanisms for these systems from microscopic models. Although complex spin dynamics in the presence of the relevant interactions can be difficult to evaluate, these interactions can be known to a high degree of precision and irrelevant terms systematically dropped from the Hamiltonian. Indeed, for electron spin qubits confined to quantum dots in GaAs or natural Si, the dominant contribution to dephasing is known to be the Fermi contact hyperfine interaction between the electron spin and nuclear spins in the surrounding host material.¹⁻⁴

The contact hyperfine interaction divides naturally into two contributions: a secular (diagonal) part that commutes with the electron Zeeman term, for which dynamics are reversible by Hahn echo,² and a non-secular (off-diagonal) part, the so-called flip-flop interactions, which may lead to a more complex dynamics. In the presence of a large electron Zeeman splitting compared to the total hyperfine interaction strength, perturbative expansions can be used to calculate the contribution of flip-flop interactions to decoherence.^{5,6} Alternative techniques such as cluster expansions or high-order partial resummations have also been used to estimate dynamics due to flip-flops in the low-field limit.⁷⁻¹¹

In addition to hyperfine interactions, dipole-dipole coupling between nuclear spins can induce internal dynamics in the nuclear-spin bath, which can act back on the electron spin through hyperfine interactions, resulting in decoherence. This process of electron-spin decoherence due to fluctuations in the nuclear-spin bath (spectral diffusion¹²) is independent of the applied magnetic field for moderately large fields and is not fully reversible by spin-echo,^{13,14} thereby typically limiting achievable coherence times.

Electron spins confined in silicon using either quantum

dots⁴ or at single phosphorus donors^{15,16} may have significant advantages over spins in GaAs quantum dots, since natural silicon contains only 4.7% nuclear-spin-carrying ²⁹Si, a figure that can be further reduced by isotopic purification.

Although the long coherence times achievable for semiconductor spin qubits are certainly an advantage, control and scalability are also required for potential applications in quantum information processing. A useful tool in this respect is a magnetic-field gradient. Indeed, electron-spin resonance of single electron spins in lateral dots in GaAs has been demonstrated using inhomogeneous magnetic fields generated by cobalt micromagnets.^{17,18} Recent proposals suggest to use these gradients to achieve strong coupling of single electron spins to a coplanar-waveguide resonator,¹⁹ in particular in Si where coherence times are longer. Interactions with a resonator can be used for a qubit readout^{20,21} or to mediate interactions between distant spin qubits,²² an important step toward scalability.

In this article, we calculate the effect of such an inhomogeneous magnetic field on the coherence of (electron or heavy-hole) spin qubits. These results can be applied to a number of experimentally relevant scenarios (see Fig. 1). We account for the secular hyperfine interaction along with the electron- and nuclear-Zeeman terms due to an inhomogeneous magnetic-field gradient. This inhomogeneity can lead to dynamics in the nuclear-spin system and a consequent decay of electron-spin coherence, similar to the case of spectral diffusion from nuclear dipolar interactions. We further show that a magnetic-field gradient can result in the failure of two typical techniques used to mitigate decoherence due to the nuclear environment: nuclear spin state narrowing and Hahn echo. State narrowing involves the preparation of the nuclear-spin bath in a narrow distribution of eigenstates of the nuclear field operator. Ideally, this corresponds to an exact eigenstate of the component of the nuclear field along an applied magnetic field.²³⁻²⁷ The presence of a transverse magnetic-field gradient destroys this dephasing-free

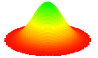
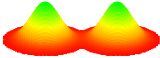

Wavefunction	Single dot	Double dot
$\psi_i(\mathbf{r}) \propto \exp\left[-\frac{1}{2}\left(\frac{ \mathbf{r}-\mathbf{r}_i }{r_0}\right)^2\right]$		
Logical spin qubit	$\{ \uparrow\rangle, \downarrow\rangle\}$	$\{ \uparrow\rangle, \downarrow\rangle\}$ or $\left\{\frac{ \uparrow\downarrow\rangle \pm \downarrow\uparrow\rangle}{\sqrt{2}}\right\}$
Wavefunction	Donor	
$\psi_i(\mathbf{r}) \propto \exp\left[-\frac{1}{2}\frac{ \mathbf{r}-\mathbf{r}_i }{r_0}\right]$		
Logical spin qubit	$\{ \uparrow\rangle, \downarrow\rangle\}$	

FIG. 1: (Color online) Various physical systems considered in this paper. We study spin dynamics for both single- and double-dot geometries. In the double-dot case, we consider either (i) a single electron shared by the two dots or (ii) an electron in each dot, with spin states expressed in the singlet-triplet basis, $\{|S\rangle = (|\uparrow\downarrow\rangle - |\downarrow\uparrow\rangle)/\sqrt{2}, |T_0\rangle = (|\uparrow\downarrow\rangle + |\downarrow\uparrow\rangle)/\sqrt{2}\}$. The associated electron envelope wavefunctions can be either hydrogenic (relevant for a donor impurity) or Gaussian (relevant for a quantum dot) in dimension $d = 1, 2$, or 3.

nuclear-spin state, leading to free-induction decay (FID) of the spin qubit. The second technique, a Hahn echo (HE), involves a refocusing pulse applied at time t after initial preparation. This procedure reverses the evolution of the spin qubit under a *static* secular hyperfine coupling, allowing for a retrieval of coherence at time $2t$. In this case, the presence of an inhomogeneous transverse magnetic field then leads to a finite nuclear-spin-bath correlation time, preventing the full recovery of spin-qubit coherence.

Our analysis of a transverse magnetic-field gradient on the decoherence dynamics of spin qubits applies to several different systems: spins in quantum dots formed in, e.g., either III-V semiconductors or Si, and to single P donor impurities in Si (Si:P) (see Fig. 1). In each case, we find that a magnetic-field gradient can decrease the coherence time, relative to known coherence times in the absence of a magnetic-field gradient. In addition to electron spins, our dephasing model is directly applicable to hole spins in III-V semiconductors,^{28–32} and may give insight into dephasing from the nuclear quadrupolar interaction due to inhomogeneous strain in InAs nanowires.³³

The remainder of this article is divided as follows. In Sec. II, we introduce the Hamiltonian accounting for Zeeman terms coupling to the spin qubit and nuclear-spin bath for an inhomogeneous magnetic field, as well as the secular hyperfine coupling. We then derive an exact formula for the spin coherence factor. In Sec. III, we introduce a perturbative method to obtain simple expressions for the coherence factor with associated parametric dependences. In Sec. IV, we obtain analytical expressions for the electron spin coherence factor in the context of free-induction decay for an initial narrowed nuclear-spin state and for Hahn echo with an initial infinite-

temperature thermal state of the nuclear-spin system. In Sec. V, we apply our model to the physical systems shown in Fig. 1 and make testable predictions for experiments that we expect to be realizable with present technology. We conclude in Sec. VI with a discussion of the most important results presented here and possible implications for future experiments on spin dynamics in these systems.

II. HAMILTONIAN AND EXACT SOLUTION

We consider a single electron spin interacting with a nuclear-spin bath through hyperfine coupling. In general, the coupling may arise from the Fermi contact term³⁴ (most relevant for electrons in III-V semiconductors), purely anisotropic interactions (relevant for, e.g., hole spins in III-V semiconductors²⁸), or both (relevant for, e.g., spins in silicon^{35,36}). We will, however, consider only the cases where spin dynamics is dominated by the secular hyperfine coupling (the part that commutes with the electron Zeeman term). We allow for a position-dependent external magnetic field $\mathbf{B}_{\text{ext}}(\mathbf{r}) = B^x(\mathbf{r})\hat{\mathbf{x}} + B\hat{\mathbf{z}}$, B being a constant, as illustrated in Fig. 2(a). We further take $\mathbf{B}_{\text{ext}}(\mathbf{r})$ and the electron envelope wavefunction $\psi(\mathbf{r})$ to satisfy $\int d^3r \mathbf{B}_{\text{ext}}(\mathbf{r})|\psi(\mathbf{r})|^2 = B\hat{\mathbf{z}}$ [this is true, e.g., when $B^x(\mathbf{r})$ is an odd function of z , while $|\psi(\mathbf{r})|^2$ is an even function of z , as in Fig. 2(a)]. As illustrated in Fig. 2(a), this means that the external magnetic field experienced by the electron is aligned with the quantum dot principal axis of symmetry, such that the g -tensor is diagonal and only its z component is relevant. Adding a secular hyperfine coupling gives⁵¹ (setting $\hbar = 1$),

$$\hat{H} = (b + \hat{h}^z)\hat{S}^z + \sum_k \gamma_k \left(b_k^x \hat{I}_k^x + b \hat{I}_k^z \right), \quad (1)$$

where $\hat{h}^z = \sum_k A_k \hat{I}_k^z$ is the Overhauser field, with sums over nuclear spins k , $b = g^* \mu_B B$ is the electron Zeeman splitting, $\gamma_k b_k^x = \gamma_k g^* \mu_B B^x(\mathbf{r}_k)$, and $\gamma_k = \gamma_k^1 / g^* \mu_B$, where γ_k^1 is the nuclear gyromagnetic ratio. The nuclear gyromagnetic ratios are thus given by $\gamma_k g^* \mu_B$, with μ_B the Bohr magneton and g^* the effective g -factor. Finally, $A_k \propto |\psi(\mathbf{r}_k)|^2$ is the hyperfine coupling strength at nuclear site $k = 0, 1, 2, \dots$. These couplings are calculated as functions of k for several relevant wavefunctions in Appendix A.

Eigenstates of \hat{H} , Eq. (1), are simultaneous eigenstates of \hat{S}^z , which we denote $\{|\uparrow\rangle, |\downarrow\rangle\}$. Since there is no interaction between nuclear spins, the eigenstates of \hat{H} can further be written as a product of nuclear-spin states of definite angular momentum along the direction of an effective field \mathbf{h}_k^σ , [see Fig. 2(b)], for each nuclear spin at site k with electron spin $\sigma = \uparrow, \downarrow$. These states can be obtained from an electron-spin-state-dependent rotation $\hat{R}_k^{\uparrow/\downarrow} = e^{-i\hat{I}_k^y \phi_k^{\uparrow/\downarrow}}$ applied to I_k^z -eigenstates, $|I_k, m_k\rangle$,

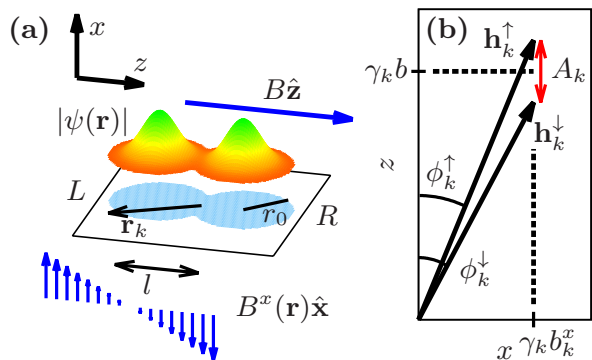


FIG. 2: (Color online) (a) Example of a device studied in this paper. A constant longitudinal magnetic field $B\hat{z}$ and an inhomogeneous transverse magnetic field $B^x(\mathbf{r})\hat{x}$ are applied to an electron spin interacting with a nuclear-spin bath. The light blue circles illustrate the range r_0 of the electron wavefunction $\psi(\mathbf{r})$ in the specific case of a double quantum dot with left ($|L\rangle$) and right ($|R\rangle$) single-particle orbital states separated by a distance l . (b) Total effective field $\mathbf{h}_k^{\uparrow/\downarrow}$ experienced by nuclear-spin k , including Knight shifts coming from the secular hyperfine interaction (of strength A_k) with the electron spin, which can be in state $|\uparrow\rangle$ or $|\downarrow\rangle$. This can be viewed as an electron-spin-dependent rotation of the nuclear spin precession axis by an angle $\phi_k^{\uparrow/\downarrow}$, which also depends on the Zeeman field $\gamma_k(b_k^x, 0, b)$. Thus, because of the inhomogeneous magnetic field, the precession axis is slightly different for each nuclear spin. This leads to a finite correlation time for collective states of the nuclear-spin bath, preventing the full recovery of electron spin coherence.

where

$$\phi_k^{\uparrow/\downarrow} = \arctan\left(\frac{\gamma_k b_k^x}{b\gamma_k \pm \frac{1}{2}A_k}\right), \quad (2)$$

as illustrated in Fig. 2(b). This gives the exact electron-spin coherence factor $C(t)$, defined by $\langle \hat{S}^+(t) \rangle = \langle \hat{S}^+(0) \rangle C(t)$, for two protocols: (i) free-induction decay and (ii) Hahn echo.

For both Hahn echo and free-induction decay, we take an initial nuclear-spin state of the form $\hat{\rho}_I(0) = \sum_{j=1}^M p_j |j\rangle \langle j|$, with $|j\rangle = \prod_k |\psi_k^j\rangle$, i.e., a statistical mixture containing M tensor-product states. In this paper, we will focus on two possible initial states: narrowed states and infinite-temperature thermal states. Narrowed nuclear-spin states are defined as a mixture of eigenstates $\{|j\rangle\}$ of \hat{h}^z having the same eigenvalue h_n^z for all j , i.e. that satisfy the equation

$$\hat{h}^z |j\rangle = h_n^z |j\rangle. \quad (3)$$

For numerical evaluation, we generate such a state by taking $|\psi_k^j\rangle = |I_k, m_k^j\rangle$ and $p_j = \delta_{jj'}$ (i.e., $M = 1$), with the eigenvalues m_k^j of \hat{I}_k^z uncorrelated for different k and chosen randomly from a uniform distribution. To evaluate thermal averages over infinite-temperature states,

we take $p_j = 1/M$ with $|\psi_k^j\rangle$ a random spin coherent state with quantization axis sampled uniformly on the unit sphere independently for each k, j . The value of M is set by increasing this value until the coherence factor has converged to within approximately 1%; we find a value $M \sim 100$ is typically sufficient for convergence.

In the case of free-induction decay, the time-evolution operator is simply $\hat{U}(t) = e^{-i\hat{H}t}$ and the coherence factor is given by $C(t) = \sum_j p_j C_j(t)$, with

$$C_j(t) = \prod_k \langle \psi_k^j | \hat{R}_k^\dagger [\hat{E}_k^\dagger(t)]^\dagger \hat{Q}_k^\downarrow \hat{E}_k^\downarrow(t) (\hat{R}_k^\downarrow)^\dagger | \psi_k^j \rangle, \quad (4)$$

and where we have introduced $\hat{Q}_k^{\uparrow/\downarrow} = e^{-i\hat{I}_k^y(\phi_k^{\uparrow/\downarrow} - \phi_k^{\downarrow/\uparrow})}$ and

$$\hat{E}_k^{\uparrow/\downarrow}(t) = \sum_{m_k=-I_k}^{I_k} e^{-im_k h_k^{\uparrow/\downarrow} t} |I_k, m_k\rangle \langle I_k, m_k|, \quad (5)$$

$$h_k^{\uparrow/\downarrow} = \sqrt{(\gamma_k b_k^x)^2 + (b\gamma_k \pm A_k/2)^2}. \quad (6)$$

In the case of Hahn echo, a refocusing pulse (a π -pulse, with unitary given by the Pauli matrix $\hat{\sigma}^x$) is applied at time t , and again at time $2t$ to return the spin to its initial state. Thus, the time-evolution operator is given by $\hat{U}(2t) = e^{-i\hat{\sigma}^x \hat{H} \hat{\sigma}^x t} e^{-i\hat{H}t}$ and the electron-spin coherence factor is

$$C_j(2t) = \prod_k \langle \psi_k^j | \hat{R}_k^\dagger (\hat{E}_k^\dagger)^\dagger \hat{Q}_k^\downarrow (\hat{E}_k^\downarrow)^\dagger \hat{Q}_k^\uparrow \hat{E}_k^\uparrow \hat{Q}_k^\downarrow \hat{E}_k^\downarrow (\hat{R}_k^\downarrow)^\dagger | \psi_k^j \rangle. \quad (7)$$

Note that we have dropped the explicit t -dependence on $\hat{E}_k^{\uparrow/\downarrow}$ in Eq. (7).

Knowing the distribution of hyperfine couplings, magnetic-field distribution, and gyromagnetic ratios for the nuclear spins, Eqs. (4) and (7) can be used to compute the exact electron-spin coherence factor numerically. The calculation involves a product of $\mathcal{O}(N)$ square matrices of dimension $2I+1$, N being the number of nuclear spins within r_0 , the effective (donor or quantum-dot) Bohr radius. Therefore, for large systems with $\gtrsim 10^6$ nuclear spins, the computation time can become rather long. More importantly, Eqs. (4) and (7) do not give any physical insight into the coherence time of the electron spin with respect to relevant physical parameters. For these two reasons, in the rest of this paper, we seek approximate expressions for the coherence factor which have a simpler form.

III. SIMPLIFIED COHERENCE FACTOR

In this section, we approximate $C(t)$ using a Magnus expansion. The Magnus expansion is a perturbation theory in the amplitude of Knight-shift fluctuations $\sim A_k$ relative to the typical rate of nuclear-spin fluctuations $\sim \omega_k = \gamma_k \sqrt{b^2 + (b_k^x)^2}$. We will be able to truncate the expansion for the time-evolution operator at leading

order in $A_k/\omega_k \ll 1$, giving expressions for both free-induction decay and Hahn echo. In addition, we will invoke a Gaussian approximation, valid for a large uncorrelated nuclear-spin bath, to obtain simple approximate expressions for the coherence factor. We ultimately show that, at leading order in the Magnus expansion, the coherence factor for a nuclear-spin bath in a narrowed state is only affected by fluctuations of transverse components of the nuclear field, \hat{h}_x, \hat{h}_y , whereas all components ($\hat{h}_x, \hat{h}_y, \hat{h}_z$) are equally important for an infinite-temperature thermal state. This approach generalizes that applied in the recent work of Ref. 32 on hole-spin dynamics.

A. Time-evolution operators

We first move the Hamiltonian of Eq. (1), $\hat{H} = \hat{H}_0 + \hat{V}$, to the interaction picture with perturbation $\hat{V} = \hat{h}^z \hat{S}^z$ and taking \hat{H}_0 to be the Zeeman terms, yielding

$$\hat{V}(t) = e^{i\hat{H}_0 t} \hat{V} e^{-i\hat{H}_0 t} = \hat{S}^z \sum_k A_k \mathbf{v}_k(t) \cdot \hat{\mathbf{I}}_k, \quad (8)$$

$$\mathbf{v}_k(t) = [-n_k^x (\cos \omega_k t - 1), n_k^x \sin \omega_k t, (n_k^z)^2 + (n_k^x)^2 \cos \omega_k t], \quad (9)$$

where $\mathbf{n}_k = \gamma_k(b_k^x, 0, b)/\omega_k$.

In the Magnus expansion,^{37,38} the time-evolution operator is recast in the form $\hat{U}(t) = e^{-i\hat{H}_M(t)}$, where $\hat{H}_M(t)$ is given by a series expansion, $\hat{H}_M(t) = \sum_{n=0}^{\infty} \hat{H}^{(n)}(t)$. The term $\hat{H}^{(n)}(t)$ contains $n+1$ time integrals over the rapidly oscillating perturbation $\hat{V}(t)$. We therefore expect rapid convergence of the Magnus expansion in the limit of large ω_k , which sets the oscillation frequency for $\hat{V}(t)$. Explicit formulas for the lowest orders of the Magnus expansion are given in the literature.^{37,38} Criteria for the convergence of the Magnus expansion are discussed for specific physical systems considered here in Appendix C.

At leading order in the Magnus expansion, $\hat{U}(t) \simeq e^{-i\hat{H}^{(0)}(t)}$. As will be shown below, this leading-order analysis is sufficient to describe the dynamics of the coherence factor in several different spin systems. In the case of free-induction decay,

$$\hat{H}^{(0)}(t) = \int_0^t \hat{V}(t_1) dt_1 = \hat{S}^z \sum_k \mathbf{h}_k^{\text{FID}}(t) \cdot \hat{\mathbf{I}}_k, \quad (10)$$

$$\mathbf{h}_k^{\text{FID}}(t) = A_k \left[n_k^x n_k^z \left(t - \frac{\sin \omega_k t}{\omega_k} \right), n_k^x \frac{1 - \cos \omega_k t}{\omega_k}, (n_k^z)^2 t + (n_k^x)^2 \frac{\sin \omega_k t}{\omega_k} \right]. \quad (11)$$

For Hahn echo, π -pulses are applied at times t and $2t$, leading to $\hat{S}^z \rightarrow \hat{\sigma}^x \hat{S}^z \hat{\sigma}^x = -\hat{S}^z$. Therefore,

$$\hat{H}^{(0)}(2t) = \hat{S}^z \sum_k A_k \hat{\mathbf{I}}_k \cdot \left[\int_0^t \mathbf{v}_k(t_1) dt_1 - \int_t^{2t} \mathbf{v}_k(t_1) dt_1 \right] = \hat{S}^z \sum_k \mathbf{h}_k^{\text{HE}}(t) \cdot \hat{\mathbf{I}}_k, \quad (12)$$

$$\mathbf{h}_k^{\text{HE}}(t) = \frac{A_k b_k^x}{\omega_k^2} [n_k^z f_k^z(t), -f_k^y(t), -n_k^x f_k^z(t)], \quad (13)$$

$$\text{where } f_k^y(t) = 2 \cos \omega_k t - \cos 2\omega_k t - 1, \quad f_k^z(t) = \sin 2\omega_k t - 2 \sin \omega_k t. \quad (14)$$

In both cases (free-induction decay and Hahn echo), we have found an approximate evolution operator of the form $\exp[-i\hat{S}^z \hat{X}(t)]$, where $\hat{X}(t) = \sum_k \mathbf{h}_k(t) \cdot \hat{\mathbf{I}}_k$ has the simple form of independent time-varying effective fields $\mathbf{h}_k(t)$ on each nuclear spin. As expected, if $b_k^x = 0 \forall k$, $\mathbf{h}_k^{\text{FID}}(t)$ fluctuates only along \hat{z} , resulting in pure dephasing on a time scale T_2^* for a random initial nuclear-spin state. This decay will not occur, however, if the nuclear bath is initially in a narrowed state. For the ide-

ally narrowed initial state defined by Eq. (3), dephasing will arise entirely from the transverse components, $h_k^{x,\text{FID}}(t), h_k^{y,\text{FID}}(t)$, in the presence of finite b_k^x . Finally, for Hahn echo, the evolution operator only deviates from the identity for non-zero values of b_k^x .

B. Gaussian approximation and finite-size effects

The steps taken above have allowed us to obtain a simpler approximate evolution operator in the interaction picture. Nevertheless, applying this simplified evolution operator to find the coherence factor $C(t)$ typically leads to complicated expressions, especially for the case of large nuclear spin, $I > 1/2$. Therefore, we will take advantage of the large number of nuclear spins usually present in semiconductor devices to introduce the Gaussian approximation.

We will use the same symbol, $\hat{H}^{(0)}(\tau)$, for the leading-order term in the Magnus expansion for both Hahn echo and free-induction decay. For the case of free-induction decay, we take $\tau = t$ and for Hahn echo, $\tau = 2t$. The transverse spin is then given by

$$\langle \hat{S}^+(\tau) \rangle = e^{i\phi(\tau)} \langle e^{iL_0(\tau)} \hat{S}^+ \rangle, \quad (15)$$

where $\phi(\tau) = b\tau$ for free-induction decay and $\phi(\tau) = 0$ for Hahn-echo. We have also introduced $L_0(t)\hat{O} = [\hat{H}^{(0)}(\tau), \hat{O}]$, i.e., $L_0(t)$ is the Liouvillian superoperator associated with $\hat{H}^{(0)}(\tau)$. In both Eqs. (10) and (12), $\hat{H}^{(0)}(\tau)$ has the form $\hat{H}^{(0)}(\tau) = \hat{S}^z \hat{X}(\tau)$, where $\hat{X}(\tau) = \sum_k \mathbf{h}_k(\tau) \cdot \hat{\mathbf{I}}_k$ acts only on nuclear-spin degrees of freedom. This important property allows us to calculate each power in the Taylor series expansion of $e^{iL_0(\tau)} \hat{S}^+$, giving $e^{iL_0(\tau)} \hat{S}^+ = \exp[i\hat{X}(\tau)] \hat{S}^+$. For an initial state of the form $\hat{\rho}_S(0) \otimes \hat{\rho}_I(0)$, with $\hat{\rho}_S(0)$ and $\hat{\rho}_I(0)$ respectively the initial spin-qubit and nuclear-spin states, we find $\langle \hat{S}^+(\tau) \rangle = \langle \hat{S}^+(0) \rangle C_\chi(\tau)$. This defines the coherence factor for a nuclear-spin bath initially in state $\rho_I(0) = \chi$: $C_\chi(\tau) = e^{i\phi(\tau)} \langle \exp[i\hat{X}(\tau)] \rangle_\chi$. Since dephasing arises from fluctuations in the nuclear field, we define $\delta_\chi \hat{X}(\tau) = \hat{X}(\tau) - \langle \hat{X}(\tau) \rangle_\chi = \sum_k \mathbf{h}_k(\tau) \cdot \delta_\chi \hat{\mathbf{I}}_k$, and the coherence factor becomes

$$C_\chi(\tau) = e^{i\phi(\tau)} e^{i\langle \hat{X}(\tau) \rangle_\chi} \left\langle e^{i\delta_\chi \hat{X}(\tau)} \right\rangle_\chi. \quad (16)$$

The Gaussian approximation then corresponds to taking $\langle \exp[i\delta_\chi \hat{X}(\tau)] \rangle_\chi \simeq \exp[-\frac{1}{2} \langle [\delta_\chi \hat{X}(\tau)]^2 \rangle_\chi]$. This approximation is justified when the following two conditions are met:

1. There are no correlations between nuclear spins, i.e. $\langle \delta_\chi I_{k_1}^{l_1} \delta_\chi I_{k_2}^{l_2} \rangle_\chi = \langle \delta_\chi I_{k_1}^{l_1} \rangle_\chi \langle \delta_\chi I_{k_2}^{l_2} \rangle_\chi \forall k_1 \neq k_2$, with $l_1, l_2 \in \{x, y, z\}$.
2. $N \gg 1$, where N is the number of nuclear spins within the range of the electron wavefunction.

The first condition is always met for the infinite-temperature states introduced in Section II. As will be seen later in this Section, it can also be satisfied for the ideally narrowed state defined by Eq. (3). However, the number of nuclear spins N needed to adequately satisfy the second criterion can be very large. Indeed, as discussed in Appendix D, subleading corrections to the Gaussian approximation are typically only suppressed by

$\sim \mathcal{O}(1/N^\alpha)$, with $\alpha < 1$ ($\alpha = 1/4$ for free-induction decay and $\alpha = 1/8$ for Hahn echo). Thus, non-Gaussian corrections can have an important effect in small systems such as single phosphorus donors in silicon, where $N \sim 10^2$. As will be shown in Section VB2, in situations where the Gaussian approximation predicts Gaussian ($\sim e^{-t^2}$) decay, the exact solution will rather exhibit exponential ($\sim e^{-t}$) behavior.

For the rest of this section, we assume that N is sufficiently large to avoid these finite-size effects. We can then proceed to the calculation of explicit coherence-factor formulas for each considered nuclear-spin state. We first consider an infinite-temperature thermal state, which we model as described in Section II, i.e. by a statistical mixture $\hat{\rho}_I(0) = \sum_j p_j |j\rangle \langle j|$ of M states $|j\rangle = \prod_k |\psi_k^j\rangle$, with each nuclear spin randomly oriented in space. In this state, nuclear spins are uncorrelated, justifying use of the Gaussian approximation. Calculating the moments involved in Eq. (16) and taking $M \rightarrow \infty$, we find that the only nonvanishing contributions come from $\langle (\hat{I}_k^x)^2 \rangle_{\text{th}} = \langle (\hat{I}_k^y)^2 \rangle_{\text{th}} = \langle (\hat{I}_k^z)^2 \rangle_{\text{th}} = \frac{1}{3} I_k(I_k + 1)$, and the coherence factor reduces to

$$C_{\text{th}}(\tau) \simeq e^{i\phi(\tau)} \exp \left[-\frac{1}{6} \sum_k I_k(I_k + 1) |\mathbf{h}_k(\tau)|^2 \right]. \quad (17)$$

Thus, for an infinite-temperature thermal state, all components of the nuclear field ($\hat{h}_k^x, \hat{h}_k^y, \hat{h}_k^z$) appear with the same prefactor, with each individual value of $h_k^\alpha(\tau)$ set by the field distribution and coherence measurement scheme (free-induction decay or Hahn echo).

By definition, an ideally narrowed state $\hat{\rho}_n$ satisfies Eq. (3). Most generally, this state can be written as $\hat{\rho}_n = \sum_j p_j |j\rangle \langle j| + \sum_{i \neq j} \rho_{ij} |i\rangle \langle j|$, where the sums are performed over all the degenerate eigenstates $|j\rangle$ of \hat{h}^z with energy h_n^z . We can then use the fact that $C_n(\tau) = e^{i\phi(\tau)} \langle \exp[i\hat{X}(\tau)] \rangle_n = e^{i\phi(\tau)} \sum_j p_j C_j(\tau) + e^{i\phi(\tau)} \sum_{i \neq j} \rho_{ij} C_{ij}(\tau)$, where $C_j(\tau) = \langle \exp[i\hat{X}(\tau)] \rangle_j$ and $C_{ij}(\tau) = \langle j | \exp[i\hat{X}(\tau)] | i \rangle$. Assuming no special phase relationship between the eigenstates $|j\rangle$, we can drop the second term in $C_n(\tau)$, which amounts to dropping the coherences in $\hat{\rho}_n$.⁶ Then, for each tensor-product state $|j\rangle = \prod_k |I_k, m_k^j\rangle$, nuclear-spin fluctuations on different sites are uncorrelated (i.e., $\langle \delta_j \hat{I}_k^z \delta_j \hat{I}_{k'}^z \rangle_j \propto \delta_{k,k'}$), so we apply the Gaussian approximation to calculate each $C_j(\tau)$. We further find that all the moments involved vanish in each state $|j\rangle$, except for $\langle \hat{I}_k^z \rangle_j$, $\langle (\delta_j \hat{I}_k^z)^2 \rangle_j$, $\langle (\delta_j \hat{I}_k^y)^2 \rangle_j$, $\langle \delta_j \hat{I}_k^x \delta_j \hat{I}_k^y \rangle_j$, and $\langle \delta_j \hat{I}_k^y \delta_j \hat{I}_k^x \rangle_j$. Furthermore, we find that $\langle \delta_j \hat{I}_k^x \delta_j \hat{I}_k^y \rangle_j$ and $\langle \delta_j \hat{I}_k^y \delta_j \hat{I}_k^x \rangle_j$ cancel each other out, and that $\langle \hat{I}_k^z \rangle_j = m_k^j$ and $\langle (\delta_j \hat{I}_k^z)^2 \rangle_j = \langle (\delta_j \hat{I}_k^y)^2 \rangle_j = \frac{1}{2} [I_k(I_k + 1) - (m_k^j)^2]$. The result is further simplified for $N \gg 1$. Indeed, the number of available eigenstates $|j\rangle$ of \hat{h}^z scales exponentially with N , such that states that have isotropic distributions of m_k^j 's are overwhelmingly more probable than states for which m_k^j depends on the site k . We can thus replace every $(m_k^j)^2$ by its expectation

value⁵² $E(m^2) = \sum_m p(m)m^2$, with $p(m)$ a probability distribution over accessible values of m . Taking $p(m)$ to be uniform, we find $\langle(\delta_j I_k^x)^2\rangle_j = \langle(\delta_j I_k^y)^2\rangle_j = \frac{1}{3}I_k(I_k+1)$. Inserting the calculated moments in Eq. (16) and considering a single realization j of a narrowed state, we obtain

$$C_n(\tau) \simeq e^{i\phi_n(\tau)} \exp\left[-\frac{1}{6}\sum_k I_k(I_k+1)|\mathbf{h}_k^\perp(\tau)|^2\right], \quad (18)$$

where $\mathbf{h}_k^\perp(\tau)$ is the projection of $\mathbf{h}_k(\tau)$ in the $x-y$ plane and $\phi_n(\tau) = \phi(\tau) + \frac{h_z^n}{A}\sum_k h_k^z(\tau)$, with $h_z^n = \langle j|\hat{h}^z|j\rangle = \sum_k A_k m_k^j$. Strikingly, $h_k^z(\tau)$ appears only in the phase $\phi_n(\tau)$, and therefore does not contribute to the decay of the coherence factor. This is a direct consequence of the vanishing variance in \hat{h}_z for a narrowed state.

IV. COHERENCE MEASUREMENT PROTOCOLS

In the previous section, we found compact expressions for $C(\tau)$ for a nuclear-spin bath initially in an infinite-temperature thermal or narrowed state. We now use these results to obtain characteristic features of the coherence dynamics under a magnetic-field gradient. In other words, we replace $\mathbf{h}_k(\tau) \rightarrow \mathbf{h}_k^{\text{FID}}(\tau)$ for free-induction decay and $\mathbf{h}_k(\tau) \rightarrow \mathbf{h}_k^{\text{HE}}(\tau)$ for Hahn echo. In each case, we study both short-time and long-time behavior. We first consider free-induction decay for an initially narrowed nuclear-spin state and show that at long time ($t \gtrsim \max[1/\gamma\Delta b^x, 1/\gamma b]$, with Δb^x the typical range of b_k^x experienced within the envelope wavefunction), the coherence factor decays as a Gaussian, $C(t) \sim \exp[-(t/T_2^\nabla)^2]$. We then address the case of Hahn-echo decay with infinite-temperature thermal states. Although for short times, we find the Hahn-echo decay envelope to be of the form $\sim \exp[-(t/T_{2e}^\nabla)^4]$, for long times coherence dynamics is very rich, displaying revivals, incomplete decay due to motional averaging, or exponential decay (reflecting a Markovian limit), depending on the particular physical setting and associated parameters.

A. Free-induction decay with narrowed states

Substituting Eq. (11) for $\mathbf{h}_k(\tau)$ into Eq. (18), which gives the coherence factor for a bath initially in a narrowed state, we obtain

$$C_n(t) \simeq e^{i\phi_n(t)} \exp\left[-\sum_k \frac{I_k(I_k+1)}{6} A_k^2 (n_k^x)^2 g_k(t)\right], \quad (19)$$

$$g_k(t) = (n_k^z)^2 \left(t - \frac{\sin \omega_k t}{\omega_k}\right)^2 + \left(\frac{1 - \cos \omega_k t}{\omega_k}\right)^2. \quad (20)$$

The term that grows as $\sim t^2$ in the argument of the exponential in $C(t)$ dominates for $t \gtrsim \max(1/\gamma\Delta b^x, 1/\gamma b)$, resulting in an approximate Gaussian decay,

$$C_n(t) \simeq e^{i\phi_n(t)} \exp\left[-(t/T_2^\nabla)^2\right], \quad (21)$$

$$\frac{1}{T_2^\nabla} = \frac{1}{b} \sqrt{\frac{1}{6}\sum_s \nu_s I_s (I_s + 1) \gamma_s^2 \Sigma_s^2}, \quad (22)$$

$$\Sigma_s^2 = \sum_{k_s} (b_{k_s}^x A_{k_s})^2, \quad (23)$$

where \sum_s is taken over all nuclear species s in the material, such that ν_s , I_s , and γ_s are, respectively, the relative abundance, nuclear spin, and gyromagnetic ratio of species s . We have also defined Σ_s^2 as a sum over nuclei k_s belonging to the same species s , which depends on the geometry of the magnetic field through $b_{k_s}^x$ and on the electron wavefunction through A_{k_s} . Explicit formulas for Σ_s^2 are given in Appendix E for various geometries. Thus, in this typical narrowed-state free-induction decay scenario, we find Gaussian decay with inverse decay time $1/T_2^\nabla \sim (A/\sqrt{N})(\gamma\Delta b^x/b)$. As mentioned in Section III B and as will be shown explicitly in Section V B 2, this behavior results from the Gaussian approximation, which breaks down when the number N of nuclear spins interacting with the electron spin is not sufficiently large.

B. Hahn echo

We now consider the coherence factor when the nuclear-spin bath is in an infinite-temperature thermal state. The relevant coherence factor is given by Eq. (17). Substituting $\mathbf{h}_k(t) \rightarrow \mathbf{h}_k^{\text{HE}}(t)$ from Eq. (13) into Eq. (17), we find

$$C_{\text{th}}(2t) \simeq \exp\left[-\frac{8}{3}\sum_k I_k(I_k+1) \frac{(A_k \gamma_k b_k^x)^2}{\omega_k^4} \sin^4\left(\frac{\omega_k t}{2}\right)\right]. \quad (24)$$

This sum can be simplified further in various physically meaningful cases which are discussed in this section.

The most straightforward way to reduce Eq. (24) is through a short-time approximation. Expanding $\sin^4(\omega_k t/2)$ to leading order in $\omega_k t/2$ yields

$$C_{\text{sh}}(2t) \simeq \exp\left[-(t/T_{2,e}^\nabla)^4\right], \quad (25)$$

$$\frac{1}{T_{2,e}^\nabla} = \left(\frac{1}{6}\sum_s \nu_s I_s (I_s + 1) \gamma_s^2 \Sigma_s^2\right)^{1/4}. \quad (26)$$

Thus, under the short-time approximation, decay occurs within a dephasing time $T_{2,e}^\nabla$, defined such that $C_{\text{sh}}(2T_{2,e}^\nabla) = 1/e$. As will be shown in Section V A, this dephasing mechanism can dominate other processes (electron-nuclear flip-flops and nuclear dipolar interactions), which have given rise to decay measured in GaAs

singlet-triplet qubits.^{2,5,7} In addition, we further note that a gradient in the z component of the magnetic field would have no effect on Hahn-echo dephasing. Indeed, such a gradient can easily be incorporated in our model with the simple replacement $\gamma_k b \rightarrow \gamma_k b_k^z$. Since $T_{2,e}^\nabla$ is independent of b , z gradients do not contribute; in order for a longitudinal gradient to contribute to dephasing, nonsecular terms in the hyperfine interaction would need to be included.³⁹

As in recent calculations for hole-spin echo dynamics,³² for large b , a motional-averaging regime can be reached in Hahn echo. Indeed, when $b \gg \Delta b^x$, we have $\omega_{k_s} \simeq \gamma_s b$ and then Eq. (24) predicts recurrences in the coherence factor with a period $\sim 1/\gamma_s b$. For sufficiently large $\omega_k \propto b$, Eq. (24) shows that $C(t) \sim 1$ for all time, in which case the motional-averaging regime has been reached. This occurs for $b \gtrsim b_c$, where

$$b_c = \left(\sum_s \nu_s I_s (I_s + 1) \frac{\Sigma_s^2}{\gamma_s^4} \right)^{1/4}. \quad (27)$$

Thus, while a transverse magnetic-field gradient can enhance dephasing, this enhancement can be controlled or eliminated with b large enough to reach the motional-averaging regime. In GaAs, for a single electron shared by two dots of radius $r_0 = 25$ nm separated by $l = 200$ nm with $N = 4.4 \times 10^6$ nuclei within r_0 (parameters taken from Ref. 2) with an added transverse gradient $\partial_z B^x|_{z=0} = 1$ T/ μm (a typical value from Refs. 17,18,40), we find $B_c = b_c/g^*\mu_B \sim 300$ mT. For a single dot with the same properties, we find $B_c \sim 200$ mT. To evaluate Σ_s^2 , we have used Eqs. (E3) and (E2), respectively, for double- and single-dot geometries.

Finally, when $b \ll \Delta b^x$ we replace $\omega_k \simeq \gamma_k b_k^x$ in Eq. (24). The time-dependence of the resulting sum over k then strongly depends on geometry. Therefore, we have derived explicit formulas for that sum limiting ourselves to single electrons in single and double dots in 2D, with Gaussian orbital wavefunctions. In both cases, we take b_k^x from Eq. (E1) and A_k , respectively, from Eq. (A1) or (A4) for single and double dots. Assuming an isotropic distribution of nuclear spins, we calculate an average of the sum over k appearing in Eq. (24) with respect to the angular degree of freedom in the position of each nucleus. For $t \gtrsim 1/\gamma \Delta b^x$, for single dots the decay becomes exponential, with $C_{\text{th}}(2t) = \exp(-t/T_{2\text{M}}^\nabla)$. For a Gaussian electron wavefunction, the A_k 's are given by Eq. (A1) and we obtain for $b \ll \Delta b^x$, $t \gtrsim 1/\gamma \Delta b^x$,

$$C_{\text{th}}(2t) = \exp(-t/T_{2\text{M}}^\nabla) \quad (28)$$

$$\frac{1}{T_{2\text{M}}^\nabla} = \frac{\sqrt{\pi}}{24} \sum_s \nu_s \frac{I_s(I_s + 1) A_s^2}{\gamma_s \delta b^x N}, \quad (29)$$

where A_s is the total hyperfine coupling strength for nuclear spins of species s . We have also defined $\delta b^x \equiv r_0 \partial_z b^x|_{z=0}$, the variation of b_x over the single-dot Bohr radius r_0 . This is to be distinguished from Δb^x , the

variation of b^x over the length-scale of the whole device, which becomes $\Delta b^x = l \partial_z b^x|_{z=0}$ in the case of a double dot with separation l . Thus, Eq. (29) shows that the decay process becomes Markovian, leading to a pure exponential decay of $C_{\text{th}}(t)$, when the correlation time of the nuclear-spin bath $\sim 1/\gamma \Delta b^x$ is short compared to the decay time $T_{2\text{M}}^\nabla$, i.e., when $T_{2\text{M}}^\nabla > 1/\gamma \Delta b^x$. This allows us to determine a critical field gradient, δb_{M}^x , beyond which the leading contribution to dephasing is exponential. Comparing Eqs. (25) and (29) for a homonuclear (single-isotope) spin bath, we find

$$\delta b_{\text{M}}^x = \frac{1}{2\sqrt{3}} \left(\frac{\pi}{2} \right)^{1/3} \sqrt{I(I+1)} \frac{A}{\gamma \sqrt{N}}. \quad (30)$$

Thus, we find Markovian decay when the broadening of nuclear spin precession frequencies due to the gradient $\sim \gamma \delta b_{\text{M}}^x$ exceeds the nuclear-field fluctuations $\sim A/\sqrt{N}$. This behavior is not obtained in our model for double dots. Indeed, in that geometry, all nuclei that interact significantly with the electron spin are subject to a finite magnetic field, with average value $\pm(l/2) \partial_z B^x|_{z=0}$, with l the inter-dot spacing, the sign depending on which dot a nuclear-spin occupies. Averaging over the angular degree-of-freedom and evaluating the sum in Eq. (24), we find that the double-dot geometry prevents the occurrence of a Markovian regime at long times, and that we rather have $\lim_{t \rightarrow \infty} C_{\text{th}}(2t) = C_0$, C_0 being a constant. In other words, in a double quantum dot, a very strong transverse field gradient alone can lead to motional averaging, in contrast to the single-dot case where a longitudinal field is needed. This qualitative difference in behavior between single and double dots is illustrated in Fig. 4(c).

V. PHYSICAL REALIZATIONS

In the previous sections, we have found the main features of the coherence dynamics under a magnetic-field gradient. The purpose of the present section is to predict whether these features could be measured in common materials used in current-day experiments. In particular, we find conditions under which this decoherence mechanism dominates over the leading dephasing sources known in these materials in the absence of a magnetic-field gradient. We focus on quantum dots in both GaAs and Si, and also investigate the case of single P donors in Si. Unless otherwise specified, for numerical evaluation, we have used hyperfine coupling constants and gyromagnetic ratios for the considered materials from the literature.^{41,42}

A. GaAs quantum dots

We first check how the inverse decay time, $1/T_2^\nabla$, for an initially narrowed nuclear-spin bath under a magnetic-field gradient compares with the inverse dephasing times

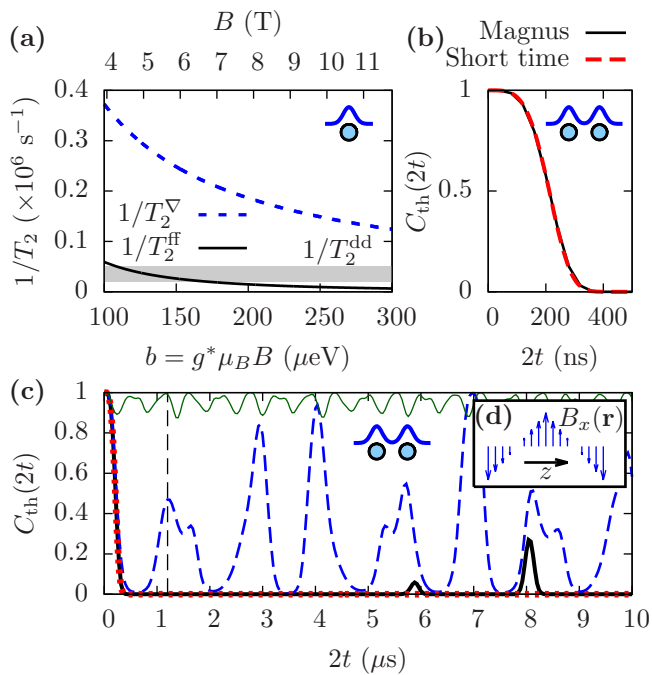


FIG. 3: (Color online) Dephasing due to a magnetic-field gradient in GaAs quantum dots. (a) Comparison of the hyperfine-induced dephasing times due to the flip-flop (T_2^{ff} , black solid line) and nuclear dipolar interactions (T_2^{dd} , gray region), with the dephasing time, T_2^{∇} , arising from the \mathbf{B} -field gradient. These times have been evaluated for FID with a bath of $N = 10^6$ nuclear spins that are prepared in a narrowed state. We consider a single electron spin in a single quantum dot with radius $r_0 = 40$ nm and $B_x(z) = z \partial_z B^x|_{z=0}$, with $\partial_z B^x|_{z=0} = 1$ T/ μm , typical for experiments.^{17,18} Solid black line: inverse dephasing time $1/T_2^{\text{ff}}$ due to flip-flop hyperfine interaction.⁵ Shaded grey area: predicted inverse dephasing times $1/T_2^{\text{dd}}$ due to nuclear dipole-dipole interactions, depending on dot size and shape.⁷ Dashed blue line: inverse dephasing time, $1/T_2^{\nabla}$, due to a magnetic-field gradient, from Eq. (22). (b) Coherence factor for infinite-temperature thermal-state HE decay in a singlet-triplet qubit with dot radii $r_0 = 25$ nm and spacing $l = 200$ nm. We also use $N = 4.4 \times 10^6$, $B = 45$ mT (parameters given in the experiment of Ref. 2), and $\partial_z B^x|_{z=0} = 0.25$ T/ μm . The transverse magnetic field has the shape illustrated in Fig. 2. We compare the full leading-order Magnus expansion of Eq. (24) (solid black line) to the short-time approximation of Eq. (25) (dashed red line). (c) Full leading-order Magnus expansion results of Eq. (24) for various B values considered in the experiment of Ref. 2: 45 mT (dotted red line), 95 mT (thick black line), 195 mT (dashed blue line), and 495 mT (thin green line). The dashed vertical line indicates the experimental dephasing time $T_{2,e}$, such that $C(2T_{2,e}) = 1/e$, measured for $B = 45$ mT in Ref. 2. Experimental dephasing times are longer for stronger magnetic fields. (d) Sawtooth-shaped transverse field distribution, for which leakage out of the S - T_0 subspace vanishes.

due to flip-flops ($1/T_2^{\text{ff}}$) and nuclear-spin dipole-dipole couplings ($1/T_2^{\text{dd}}$). $1/T_2^{\text{ff}}$ has been calculated from a Schrieffer-Wolff expansion⁵ for $b > A$, which for GaAs roughly corresponds to $B > 4$ T. The derivations of Ref. 5 result in $1/T_2^{\text{ff}} \propto 1/b^2$, while Eq. (22) predicts $1/T_2^{\nabla} \propto 1/b$. Thus, for sufficiently large b , dephasing due to the gradient will always dominate over flip-flop decay. This is illustrated in Fig. 3(a), where the dephasing rates are compared assuming typical parameters^{17,18,40} for a GaAs quantum dot and a magnetic-field gradient of 1 T/ μm . In this particular case, $1/T_2^{\nabla}$ dominates over the entire magnetic-field range considered.

In addition to flip-flops, nuclear dipolar interactions could also potentially lead to decay on a shorter time scale than the mechanisms considered here. Inverse dephasing times $1/T_2^{\text{dd}}$ due to dipole-dipole interactions have been predicted in Fig. 14 of Ref. 7 to be between 10^4 s^{-1} and 10^5 s^{-1} , with smaller values for small dot radii. For example, with a quantum-dot Bohr radius of $r_0 = 40$ nm, as in Fig. 3(a), $1/T_2^{\text{dd}}$ lies between $2 \times 10^4 \text{ s}^{-1}$ and $5 \times 10^4 \text{ s}^{-1}$ [see Fig. 3(a)] depending on the dot thickness and the crystal orientation. On the other hand, assuming $N \propto \pi r_0^2 y_0$, (where y_0 is the dot thickness), Eqs. (22) and (26) predict that $1/T_2^{\nabla}$ and $1/T_{2e}^{\nabla}$ are both independent of r_0 . Indeed, for single dots, $\Sigma^2 \sim (A\delta b^x)^2/N \sim (Ar_0\partial_z b^x)^2/N \sim 1/y_0$, with r_0 contributions canceling out. Therefore, since $1/T_2^{\text{ff}} \propto 1/N \propto 1/r_0^2$, the gradient dephasing mechanism dominates both flip-flop and dipole-dipole decay for sufficiently large dots with a fixed gradient, a situation that corresponds to the parameters of Fig. 3(a), where $1/T_2^{\nabla}$ exceeds $1/T_2^{\text{ff}}$, $1/T_2^{\text{dd}}$ by nearly an order of magnitude. Additionally, $1/T_2^{\text{dd}}$ is expected to be independent of b .¹⁴ For large dots, gradient-induced dephasing should then dominate for a wide range of b . In summary, we have the following power-law hierarchy for the various mechanisms studied here: $1/T_2^{\text{ff}} \propto 1/b^2$, $1/T_2^{\nabla} \propto 1/b$, and $1/T_{2e}^{\nabla} \propto 1$. For large dots it may then be possible to experimentally identify regimes where each mechanism dominates from a measurement of the inverse dephasing time as a function of b .

We now consider the case of GaAs singlet-triplet qubits, in which Hahn-echo dephasing dynamics without externally applied magnetic-field gradients has been extensively studied.^{2,43} As explained in Appendix B, the Hamiltonian for a system of two electron spins in the $\{|S\rangle, |T_0\rangle\} = \{(|\uparrow\downarrow\rangle - |\downarrow\uparrow\rangle)/\sqrt{2}\}, (|\uparrow\downarrow\rangle + |\downarrow\uparrow\rangle)/\sqrt{2}\}$ basis can be approximately mapped to the single-spin Hamiltonian of Eq. (1) when $b > \Delta b^x$. The results of Section IV B therefore apply equally well to the coherence of a singlet-triplet qubit [where, for a singlet-triplet qubit, $C(t)$ measures coherence between the states $|\uparrow\downarrow\rangle$ and $|\downarrow\uparrow\rangle$]. However, a finite value of $\Delta b^x \neq 0$ will typically lead to spin flips, resulting in leakage out of the $\{|S\rangle, |T_0\rangle\}$ subspace. Here, $\Delta b^x = b_R^x - b_L^x$, where $b_\alpha^x \equiv \int d\mathbf{r} g^* \mu_B B^x(\mathbf{r}) |\psi_\alpha(\mathbf{r})|^2$ and $\psi_{L(R)}(\mathbf{r})$ is a single-particle envelope function localized on the left (right) dot. The magnetic-field configuration illustrated in Fig. 2(a)

leads, for example, to $\Delta b^x \neq 0$ and consequently to finite leakage due to spin flips. One way to circumvent this leakage (as discussed below) would be to arrange a “sawtooth” magnetic-field configuration, as shown in Fig. 3(d).

We now make predictions for Hahn-echo dephasing under a magnetic-field gradient, using parameters from an experiment by Bluhm *et al.*,² in which the Hahn-echo dephasing time for a singlet-triplet spin qubit in GaAs is measured as a function of a magnetic field B , with no applied gradient, $b_k^x = 0$. We consider the effect of a weak transverse gradient $\partial_z B^x|_{z=0} = 0.25 \text{ T}/\mu\text{m}$, corresponding to $\Delta B^x = \Delta b^x/g^* \mu_B = 50 \text{ mT}$. From Eq. (27), with Σ_s^2 taken from Eq. (E4), we estimate the critical field for motional averaging to be $B_c \sim 225 \text{ mT}$. Thus, it is possible to set $\Delta B^x < B < B_c$, such that leakage outside the S - T_0 subspace remains small, but loss of electron-spin coherence due to the gradient is observed. In that regime, as illustrated in Fig. 3(b), the dynamics of the coherence factor is well-described by Eq. (25), which assumes a short-time expansion. Equation (25) predicts decay in a time $T_{2,e}^\nabla \simeq 116 \text{ ns}$, while the Hahn-echo measurements without the gradient yield a dephasing time $T_{2,e} \sim 600 \text{ ns}$ for $B = 45 \text{ mT}$. Thus, our model predicts that introducing a transverse magnetic-field gradient of only $0.25 \text{ T}/\mu\text{m}$ in that experiment would severely decrease coherence times. However, as illustrated by Fig. 3(c), taking $B \gg B_c$ would drive this system to a motional-averaging regime, avoiding rapid decay from the magnetic-field gradient.

Finally, we stress that the results of the previous paragraph correspond to a best-case scenario for the geometry of Fig. 2(a) using a singlet-triplet qubit, where all leakage out of the computational subspace has been neglected. With the magnetic-field distribution $B^x(\mathbf{r})$ of Fig. 2(a), there would be no leakage due to spin flips for a bonding/antibonding molecular state $\psi_\pm(\mathbf{r})$ with equal weight on right and left dots, chosen such that $\int d^3r |\psi_\pm(\mathbf{r})|^2 B^x(\mathbf{r}) = 0$. For an electron in one of the states $\psi_\pm(\mathbf{r})$, $T_{2,e}^\nabla$ and B_c would be comparable to the values obtained above assuming localized states in the left/right dot, $\psi_{L,R}(\mathbf{r})$. Alternatively, localized orbital states $\psi_{L,R}(\mathbf{r})$ combined with the sawtooth field distribution $B^x(\mathbf{r})$ of Fig. 3(d) would also avoid leakage provided $\int d^3r |\psi_{L,R}(\mathbf{r})|^2 B^x(\mathbf{r}) = 0$.

B. Silicon

We now apply our model to electron-spin qubits in Si, considering quantum dots and single P donors. Mainly because the density of nuclear spins is much lower than in GaAs, the hyperfine field in Si is much smaller. Indeed, in natural Si, which contains 4.7% ^{29}Si nuclei, we typically have^{4,42,44} $A \sim 100 \text{ neV}$. Without a magnetic-field gradient, for the isotopic concentration of natural silicon, Witzel *et al.* (see Fig. 23 of Ref. 45) have calculated a Hahn-echo dephasing time $T_{2,e}$ be-

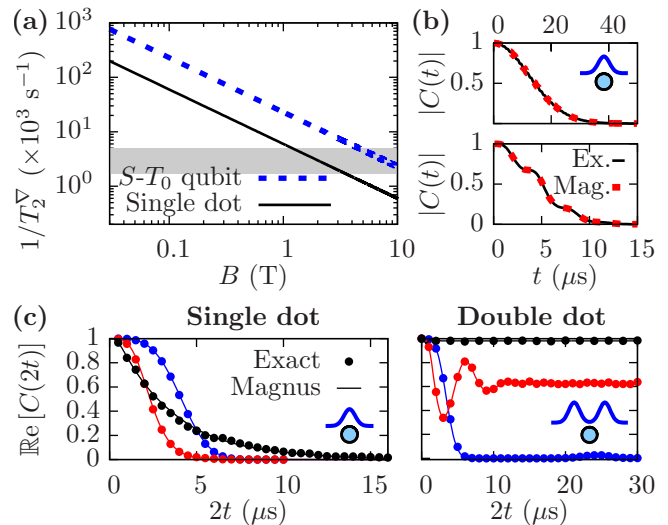


FIG. 4: (Color online) Dephasing due to a magnetic-field gradient in Si quantum dots. (a) Inverse decay times for narrowed-state FID from Eq. (22). We take a magnetic-field gradient $\partial_z B^x|_{z=0} = 1 \text{ T}/\mu\text{m}$ and a quantum-dot Bohr radius $r_0 = 15 \text{ nm}$, with inter-dot spacing $l = 80 \text{ nm}$ in the double-dot case. We also take a total hyperfine coupling $A = 210 \text{ neV}$ and $N = 10^4$ from Refs. 4,42. Shaded gray area: range of total HE inverse dephasing times $2T_{2,e}$ in Si without a magnetic field gradient.⁴⁵ (b) Coherence dynamics for narrowed-state FID in a single dot. Top: $B = 100 \text{ mT}$, bottom: $B = 30 \text{ mT}$. Dashed red line: Magnus expansion results, from Eq. (19), solid black line: exact solution, from Eq. (4). (c) Coherence dynamics for infinite-temperature thermal-state HE, with $B \rightarrow 0$. Solid lines: Magnus expansion prediction, from Eq. (24). Dots: exact solution, from Eq. (7). Blue: $\Delta B^x = 20 \text{ mT}$, red: $\Delta B^x = 80 \text{ mT}$, black: $\Delta B^x = 400 \text{ mT}$, with $\Delta B^x = \Delta b^x/g^* \mu_B$ and Δb^x defined in Section IV A.

tween 100 and 300 μs in both quantum dots and single donors (including hyperfine interaction and dipole-dipole couplings). These values are also supported by experiments performed on phosphorus-doped silicon at low concentration.^{46,47} Neglecting dipole-dipole and flip-flop interactions, our model predicts dephasing times due to a moderate magnetic-field gradient that are shorter than this 100- μs timescale. We will therefore neglect contributions to dephasing from flip-flop and dipolar interactions in the remainder of this section, focusing on the dominant magnetic-field-gradient mechanism.

1. Silicon quantum dots

We first discuss results for narrowed-state free-induction decay. Fig. 4(a) shows $1/T_{2,e}^\nabla$ as predicted from Eq. (22) for B ranging from 30 mT to 10 T. For $B < 100 \text{ mT}$ and for the parameters described in the caption of Fig. 4, $T_{2,e}^\nabla$ is smaller than 10 μs , i.e. at least an order of magnitude shorter than $2T_{2,e}$ taken from

Ref. 45, illustrated by the shaded gray area. However, for $B > 1$ T, T_2^∇ can be pushed beyond 100 μs , providing a way to avoid most of this additional dephasing. Fig. 4(b) shows the coherence dynamics of a spin in a single quantum dot. Interestingly, for $b \sim \delta b^x$ (with $\delta b^x \equiv r_0 \partial_z b^x|_{z=0}$), the result deviates from pure Gaussian ($\sim e^{-t^2}$) behavior. The coherence factor $C(t)$ displays additional envelope modulations at the nuclear-spin precession frequency, $\sim \gamma b$. This effect is illustrated in the lower plot of Fig. 4(b). The agreement between the Magnus expansion and the exact solution is very good and even reproduces these small oscillations. Precise conditions for the validity of the Magnus expansion are derived in Appendix C. We find qualitatively similar results to those presented in Fig. 4(b) for a single spin in a double dot.

Because of the smallness of A in silicon, the critical gradients required for both motional averaging and exponential decay in HE decay that were obtained in Section IV B are much smaller than in GaAs. Indeed, for a single dot, exponential decay from the onset of a Markovian regime would require $\delta b^x/g^*\mu_B > \delta b_M^x/g^*\mu_B \simeq 2$ T in GaAs, while in silicon such a regime is obtained for $\delta b^x/g^*\mu_B > \delta b_M^x/g^*\mu_B \simeq 20$ mT. Since flip-flop interactions are negligible in silicon dots even for $B \sim 1$ mT, a transition from the non-Markovian to the Markovian regime could, in principle, be observed by tuning $\delta b^x/g^*\mu_B$ from ~ 20 mT to a value > 100 mT, as illustrated in the left plot of Fig. 4(c), though sustaining such a large gradient on a length-scale of ~ 15 nm may pose a challenge with current technology. Additionally, the right-hand-side plot of Fig. 4(c) shows that, consistent with Section IV B, the coherence properties of a double dot in the long-time limit are radically different from those of a single dot. Indeed, for large ΔB^x , rather than reaching a Markovian regime, the gradient can induce motional averaging. Both the single- and double-dot calculations shown here are performed with $B = 0$ to emphasize that the gradient itself is the source of that behavior, though calculations for a small but finite field of $B \sim 1$ mT (required to justify the secular-hyperfine coupling assumption) give similar results.

2. Phosphorus donors in silicon

We now turn to single phosphorus donor spin qubits in silicon^{15,16,48} (Si:P). In this system, the logical qubit is the spin of a single electron bound to the phosphorus atom. The P nucleus has a finite spin $I = 1/2$. When b is much larger than the strength of the coupling between the electron spin and the donor nuclear spin, A_{SI} , the system is well-described by the Hamiltonian of Eq. (1). The relevant crossover magnetic field is $A_{\text{SI}}/(g^*\mu_B) \sim 1$ mT, which can be achieved with a moderate applied magnetic field.⁴⁸

First, we calculate the evolution of coherence in narrowed-state FID. As shown in Fig. 5(a), Eq. (19)

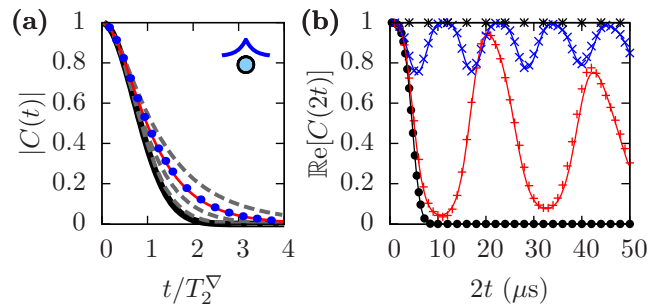


FIG. 5: (Color online) Coherence dynamics of an electron spin qubit in a single P donor in Si. We take $N = 250$, $A = 210$ neV, and $\partial_z B_x|_{z=0} = 1$ T/ μm . The system corresponds to a single dot with $r_0 = 3$ nm, $d = 3$ and $q = 1$. (a) Narrowed-state FID with $B = 200$ mT. Thick black curve: prediction from the Magnus expansion under the Gaussian approximation, Eq. (19). Thin red curve: exact solution from Eq. (4). Blue dots: Magnus expansion without Gaussian approximation, from Eq. (32). Gray dashed lines, from top to bottom: exact coherence decay, respectively, for $N = 125$, 500, and 2000. (b) Hahn-echo decay with initial thermal states for $N = 250$, with varying B . From bottom to top: $B = 0, 10$ mT, 20 mT and 100 mT. Points: exact solution of Eq. (7). Solid lines of corresponding color: prediction from the Magnus expansion, Eq. (24).

(solid black line) predicts Gaussian decay with time constant $T_2^\nabla \simeq 65$ μs , much smaller than $2T_{2,e} \sim 600$ μs ⁵³ measured in the absence of a magnetic-field gradient.^{46,47} However, the corresponding exact solution, calculated from Eq. (7) and illustrated by the red line deviates from a Gaussian in the long-time limit. Indeed, after a short-lived Gaussian-dominated behavior, the exact solution exhibits an exponential tail. Yet, according to Eq. (C7), the Magnus expansion should converge rapidly for up to $\delta B^x = \delta b^x/g^*\mu_B \sim 600$ mT, which is overwhelmingly larger than $\delta B^x = 3$ mT, as chosen here. We thus turn to the other approximation introduced in the derivation of Eq. (19): the Gaussian approximation.

To rigorously check that non-Gaussian contributions are responsible for this divergence in behavior, we notice that for $I = \frac{1}{2}$, which is the case for a bath of ²⁹Si nuclei, the exponential in Eq. (16), $e^{i\delta_x \hat{X}(\tau)}$, can be expanded using the identity

$$e^{i\mathbf{v} \cdot \hat{\sigma}} = \cos v + i \frac{\mathbf{v} \cdot \hat{\sigma}}{v} \sin v, \quad (31)$$

where \mathbf{v} is an arbitrary vector and $\hat{\sigma}$ is the vector of Pauli matrices ($\hat{\sigma}^x, \hat{\sigma}^y, \hat{\sigma}^z$). Doing so, the coherence factor can be expressed as a product,

$$C_j(t) = e^{ibt+i \sum_k h_k^z m_k^j} \prod_{k=1}^{\infty} \left(\cos \frac{|\mathbf{h}_k|}{4} + 4i \frac{h_k^z m_k^j}{|\mathbf{h}_k|} \sin \frac{|\mathbf{h}_k|}{4} \right). \quad (32)$$

We thus find an expression for the coherence factor under the leading-order Magnus expansion that includes non-Gaussian corrections if we replace $\mathbf{h}_k(t)$ by its value given

in Eq. (11). The result for single donors is given by the blue dots in Fig. 5(a). Strikingly, the leading-order Magnus expansion overlaps with the exact solution, clearly showing the breakdown of the Gaussian approximation for small nuclear-spin baths.

Though finding a criterion for the validity of the Gaussian approximation directly from Eq. (32) is not a straightforward task, an order-of-magnitude estimate is sufficient here. As explained in Appendix D, non-Gaussian corrections are suppressed only as a weak power of N ($\sim 1/N^{1/4}$). Thus, N must be fairly large for the Gaussian approximation to work, a few hundreds typically not being sufficient. Indeed, for $N = 250$, we have $N^{1/4} \simeq 3.97 \sim 1$. As illustrated by the dashed gray lines in Fig. 5, as N increases, the exponential tail due to the non-Gaussian corrections fades away, with dephasing becoming almost entirely Gaussian for $N \sim 2000$. To generate this plot, as N is increased, we have adjusted A to keep the ratio $N^{5/6}\gamma b/A$ constant, such that the criterion for convergence of the Magnus expansion expressed by Eq. (C7) remains satisfied.

Finally, Fig. 5(b) gives the evolution of the coherence factor under Hahn echo for a nuclear-spin bath initially in an infinite-temperature thermal state. From Eq. (27), we find that the critical magnetic field for the onset of motional averaging is $B_c \sim 19$ mT. This is confirmed by the exact solution of Eq (7), as shown by the points in Fig. 5(b). In past experiments,¹⁶ an external field $B \sim 1$ T has been used. For magnetic-field gradients of ~ 1 T/ μm , these experiments would be deep in the motional averaging regime, making dephasing due to the magnetic-field gradient completely reversible by Hahn echo. On a separate note, for Hahn echo, the predictions from the combination of Magnus expansion and Gaussian approximation closely fit with the exact solution, as illustrated by the solid lines. This does not contradict the results of Appendix D, since the criteria found there are sufficient but not necessary conditions for non-Gaussian contributions to be negligible.

Finally, from Eq. (24), we obtain a criterion for Markovian Hahn-echo decay due to a magnetic-field gradient that is very similar to Eq. (30), except that A_k values are taken for $d = 3$, $q = 1$. We find that Markovian behavior in single donors requires $\delta B^x \sim 100$ mT. With $r_0 = 3$ nm, this would require a gradient $\partial_z B^x|_{z=0} > 30$ T/ μm , which could be technically very difficult to achieve. Larger quantum dots such as those discussed in Section V B 1 would thus be more appropriate to observe that behavior.

VI. CONCLUSIONS

We have calculated the free-induction decay and Hahn-echo dynamics of an electron spin interacting with a nuclear-spin bath in the presence of an inhomogeneous magnetic field. Accounting for only secular hyperfine coupling, we have given exact solutions for spin coherence

in terms of a product of $\mathcal{O}(N)$ matrices. Additionally, we have found closed-form simple analytical expressions within a leading-order Magnus expansion and Gaussian approximation.

In the case of free-induction decay, the coherence factor typically decays as $\sim e^{-t^2}$. In the case of Hahn echo, we have found $\sim e^{-t^4}$ dephasing if the longitudinal magnetic field is below a known threshold, $B \lesssim B_c$, above which this system enters a motional-averaging regime characterized by an incomplete decay of spin coherence. For electron spins in single quantum dots, a large transverse magnetic-field gradient decreases the nuclear-spin correlation time, leading to Markovian (exponential) rather than $\sim e^{-t^4}$ echo dephasing. In contrast, for spins in double quantum dots we rather obtain motional averaging and an associated incomplete coherence decay in the limit of a large uniform magnetic-field gradient.

We have further investigated the relevance of the above results to three physical systems: quantum dots in GaAs or Si and single P donors in Si. In each case, the inverse dephasing time due to the magnetic-field gradient mechanism $1/T_2^\nabla$ can be much larger than those due to electron-nuclear flip-flop ($1/T_2^{\text{ff}}$) and nuclear dipole-dipole interactions ($1/T_2^{\text{dd}}$), i.e. $1/T_2^\nabla \gg 1/T_2^{\text{ff}}, 1/T_2^{\text{dd}}$. This dominance of $1/T_2^\nabla$ can be confirmed in GaAs singlet-triplet qubits [see Fig. 3(c)]. Additionally, we have found that single quantum dots in Si would be best suited to observe a cross-over between non-Markovian and Markovian dephasing. Finally, we have shown that the Gaussian approximation fails to correctly predict decoherence in small systems such as single P donors in Si. This result highlights the difference between spin baths and bosonic baths, for which Wick's theorem allows for exact suppression of all non-Gaussian contributions.

The model developed here applies directly to heavy-hole spin qubits, for which flip-flop terms can be suppressed through confinement and the secular-hyperfine limit can be reached even for very weak external magnetic fields.³² Our results may also give insight into dephasing in spin-orbit qubits in InAs nanowires,³³ where strain leads to inhomogeneous nuclear quadrupolar interactions that may decorrelate the nuclear-spin system as in the case of a magnetic-field gradient.

Acknowledgments

We thank M. Pioro-Ladrière and X. Wang for useful discussions. We acknowledge financial support from NSERC, CIFAR, FRQNT, INTRIQ, and the W. C. Sumner Foundation.

Appendix A: Hyperfine coupling constants in a double quantum dot

In this Appendix, we obtain expressions for the hyperfine coupling strengths A_k for three possible geometries:

(i) one electron in a single dot; (ii) one electron in the (bonding or antibonding) delocalized molecular state of a symmetric double quantum dot; (iii) two electrons in a double quantum dot (each in the localized $|L\rangle$ and $|R\rangle$ states), in the S - T_0 basis. Fig. 2 helps to visualize the problem in two dimensions.

Case (i) has already been treated in the literature,⁵ yielding for an electron wavefunction of the form $\psi(r) = \psi(0) \exp[-(r/r_0)^q/2]$, in dimension d ,

$$A_k = Av_0 |\psi(\mathbf{r}_k)|^2 = \frac{A}{N^{\frac{d}{q}} \Gamma\left(\frac{d}{q}\right)} e^{-(k/N)^{q/d}}, \quad (\text{A1})$$

with v_0 the volume per nuclear spin and N the number of nuclei within the dot radius r_0 .

We deal with the two cases involving a double dot in a very similar way, using left ($\sigma = L$) and right ($\sigma = R$) basis states $\psi_\sigma(\mathbf{r}_k) = \psi(\mathbf{r}^\sigma) \exp[-(r_k^\sigma/r_0)^q/2]$, where $\mathbf{r}_k^\sigma = \mathbf{r}_k - \mathbf{r}^\sigma$ and the vectors \mathbf{r}^σ locate the center of each dot. Using spherical coordinates, $(r_k^\sigma)^2 = r_k^2 + l^2/4 + r_k l G_{d,k}^\sigma$, with

$$G_{d,k}^{L/R} = \begin{cases} \pm(-1)^k & d = 1, \\ \pm \cos \theta_k & d = 2, \\ \pm \sin \theta_k \cos \varphi_k & d = 3. \end{cases} \quad (\text{A2})$$

For $d = 2$, θ_k is the polar angle that locates the nuclear spin k , while for $d = 3$, θ_k and φ_k are, respectively, the polar and azimuthal angles. As in Ref. 5, we define N as the number of nuclear spins within the Bohr radius r_0 and label the spins in increasing order of r_k , such that $r_k/r_0 = (k/N)^{1/d}$. Thus, for an electron in dot σ , the hyperfine couplings are given by

$$A_k^\sigma = A_0^\sigma \exp \left\{ - \left[\left(\frac{k}{N} \right)^{2/d} + \eta^2 + 2\eta \left(\frac{k}{N} \right)^{1/d} G_{d,k}^\sigma \right]^{q/2} \right\}, \quad (\text{A3})$$

with $\eta \equiv l/2r_0$, the dimensionless separation of the double dot, and A_0^σ is obtained from the normalization condition $\sum_k A_k^\sigma = A$.

In the case of a single electron shared by two dots of the same size and at the same electrical potential, the electron wavefunction is $\psi_\pm(\mathbf{r}) = \frac{1}{\sqrt{2}}[\psi_L(\mathbf{r}) \pm \psi_R(\mathbf{r})]$, treating both symmetric (+) and antisymmetric (-) superpositions at the same time. In order to calculate A_0^\pm and thus obtain A_k^\pm , we assume an isotropic distribution of nuclear spins and $N \gg 1$ and evaluate $A = \sum_k A_k^\pm$ by converting \sum_k to an integral to obtain for $d = q = 2$

$$A_k^\pm = Av_0 |\psi_\pm(\mathbf{r}_k)|^2 \simeq \frac{A}{N} \frac{\cosh \left(2\eta \sqrt{\frac{k}{N}} \cos \theta_k \right) \pm 1}{e^{\eta^2} \pm 1} e^{-k/N}. \quad (\text{A4})$$

In the above, we have defined A_k^\pm as the hyperfine coupling strength for nuclear spin k when the electron wavefunction is $\psi_\pm(\mathbf{r})$. As expected, A_k^\pm tends toward the single-dot expression [Eq. (A1)] for $\eta \propto l \rightarrow 0$.

Hyperfine couplings for case (iii) are obtained in a similar way, however it is first required to map the Hamiltonian of a singlet-triplet qubit to Eq. (1). This is done in Appendix B.

Appendix B: Mapping to a singlet-triplet qubit

For moderate electron Zeeman splittings $b > \Delta b^x$, the model of Eq. (1) can be applied to describe two electron spins in the S - T_0 basis,⁴⁹ defined by $|S/T_0\rangle = \frac{1}{\sqrt{2}}(|\uparrow\downarrow\rangle \mp |\downarrow\uparrow\rangle)$. Indeed, defining $\hat{\tau}_x = |S\rangle\langle T_0| + |T_0\rangle\langle S|$ and $\hat{\tau}_z = |T_0\rangle\langle T_0| - |S\rangle\langle S|$ and assuming a negligible exchange coupling, the effective Hamiltonian describing the two electron spins and their nuclear-spin bath in a magnetic-field gradient is

$$\hat{H}_{ST_0} = \hat{H}_Z^z + \hat{H}_Z^x + \delta \hat{h}^z \hat{\tau}^x + b \sum_k \gamma_k \hat{I}_k^z + \sum_k \gamma_k b_k^x \hat{I}_k^x, \quad (\text{B1})$$

where \hat{H}_Z^α is the Zeeman coupling of the electrons for a magnetic field along direction α . Defining $|T_+\rangle = |\uparrow\uparrow\rangle$ and $|T_-\rangle = |\downarrow\downarrow\rangle$, we find

$$\hat{H}_Z^z = b(|T_+\rangle\langle T_+| - |T_-\rangle\langle T_-|), \quad (\text{B2})$$

$$\hat{H}_Z^x = b^x \frac{|T_+\rangle + |T_-\rangle}{\sqrt{2}} \langle T_0| - \frac{\Delta b^x}{2} \frac{|T_+\rangle - |T_-\rangle}{\sqrt{2}} \langle S| + \text{H.c.},$$

where $b^x \equiv (b_R^x + b_L^x)/2$, $\Delta b^x \equiv b_R^x - b_L^x$ and b_i^x is the electron Zeeman splitting along x in the localized orbital state of dot i . For a magnetic field $B^x(z)$ that is an odd function of z , as shown in Fig. 2, $b^x = 0$. The term $\propto \Delta b^x$ above typically does not vanish, and thus may lead to leakage out of the S - T_0 subspace. This leakage can, however, be suppressed if $b \gg \Delta b^x$. In this limit, we neglect the term $\propto \Delta b^x$ and take $\hat{\tau}^x \rightarrow 2\hat{S}^z$ in the Hamiltonian of Eq. (B1), which approximately maps it to Eq. (1), provided we replace $A_k \rightarrow \delta A_k = A_k^L - A_k^R$. The coherence factor then corresponds to the off-diagonal element of the density matrix in the $\{|\uparrow\downarrow\rangle, |\downarrow\uparrow\rangle\}$ basis. Using the results of Appendix A, we find ($d = q = 2$)

$$\delta A_k = 2 \frac{A}{N} e^{-(\frac{k}{N} + \eta^2)} \sinh \left(2\eta \sqrt{\frac{k}{N}} \cos \theta_k \right). \quad (\text{B3})$$

We estimate corrections to the above mapping for finite Δb^x from the leakage probability, $1 - \langle \hat{P}_{ST_0}(t) \rangle$, where $\hat{P}_{ST_0} \equiv |S\rangle\langle S| + |T_0\rangle\langle T_0|$. We have evaluated $\langle \hat{P}_{ST_0}(t) \rangle$ within time-dependent perturbation theory to leading order in $\Delta b^x/b$ and A_k/ω_k . This calculation predicts the onset of a stationary leakage probability $\sim (\Delta b^x/b)^2$ after a time $\sim \sqrt{N}/A$. In principle, this probability could grow over time if other processes that can decorrelate the electron and nuclear spins were included, such as nuclear dipolar interactions. In that case, we expect the leakage probability to grow on a time scale $\sim (b/\Delta b^x)^2 \tau_c$, with τ_c the correlation time of the nuclear-spin bath. In bulk GaAs, $\tau_c \sim 100 \mu\text{s}$ can be estimated from the NMR

linewidth.⁵⁰ We therefore expect the approximate mapping to give an accurate representation of dynamics in the singlet-triplet basis for times $t \lesssim 100 \mu\text{s}$ whenever $\Delta b^x/b \lesssim 1$.

Appendix C: Validity of the Magnus expansion

Using the Gaussian approximation, we showed in Section III B that the coherence factor is of the form $C(\tau) \sim \exp[\sum_k |\mathbf{h}_k(\tau)|^2]$, as expressed in Eq. (17) and Eq. (18). The field $\mathbf{h}_k(t)$ is then obtained from the Hamiltonian of Eq. (1) with a zeroth-order Magnus expansion. To subleading order in that expansion, we would have, for $\alpha \in \{x, y, z\}$

$$(h_k^\alpha)^2 \sim \left[h_k^{\alpha(0)} \right]^2 + 2h_k^{\alpha(0)} h_k^{\alpha(2)} + \left[h_k^{\alpha(1)} \right]^2. \quad (\text{C1})$$

In the rest of this Appendix, we drop the α index to ease notation. In the above expression, $h_k^{(n)} \sim (A_k b_k^x / \omega_k)^{n+1}$, such that $h_k^{(0)} \sim (A_k b_k^x / \omega_k)^2$ is the leading term, considered in the main body of the paper, while $h_k^{(0)} h_k^{(2)}$ and $[h_k^{(1)}]^2$, of order $(A_k b_k^x / \omega_k)^4$, are subleading. Note that we have dropped terms containing odd powers of $A_k b_k^x$ because they cancel out when summed over k due to the symmetries of $|\psi(\mathbf{r})|^2$ and $B^x(\mathbf{r})$. We will now establish criteria for the leading term to dominate the subleading ones, and hence for the Magnus expansion to be valid.

The n -th order term in the Magnus expansion involves $n + 1$ integrals over time of $\mathbf{v}_k(t)$, which is given by Eq. (9). Roughly speaking, each integral of a sine generates a factor $\cos \omega_k t / \omega_k$ in $h_k^{(n)}$, while each integral of a cosine generates a factor $t \sin \omega_k t$. Thus, we find

$$h_k^{(0)} \sim \frac{\gamma A_k b_k^x}{\omega_k^2} + \frac{\gamma A_k b_k^x t}{\omega_k}, \quad h_k^{(1)} \sim \left(\frac{\gamma A_k b_k^x}{\omega_k} \right)^2 \frac{t}{\omega_k}, \quad (\text{C2})$$

$$h_k^{(2)} \sim \frac{A_k^3}{\omega_k^2} \left(\frac{\gamma b_k^x}{\omega_k} \right)^3 t + \frac{A_k^3}{\omega_k} \left(\frac{\gamma b_k^x}{\omega_k} \right)^3 t^2, \quad (\text{C3})$$

such that

$$\begin{aligned} \left[h_k^{(1)} \right]^2 + h_k^{(0)} h_k^{(2)} &\sim \frac{A_k^4}{\omega_k^3} \left(\frac{\gamma b_k^x}{\omega_k} \right)^4 t + \frac{A_k^4}{\omega_k^2} \left(\frac{\gamma b_k^x}{\omega_k} \right)^4 t^2 \\ &\quad + \frac{A_k^4}{\omega_k} \left(\frac{\gamma b_k^x}{\omega_k} \right)^4 t^3. \end{aligned} \quad (\text{C4})$$

Using an order-of-magnitude estimate of the sum over k , this gives three critical times (t_1, t_2, t_3) for which each of the above terms can be of order 1. In the limit where $b \gg \Delta b_x$, we find

$$t_1 \sim \frac{\gamma^3 N^3 b^7}{(A \Delta b^x)^4}, \quad t_2 \sim \frac{\gamma N^3 / 2 b^3}{(A \Delta b^x)^2}, \quad t_3 \sim \frac{\gamma^{1/3} N b^{5/3}}{(A \Delta b^x)^{4/3}}, \quad (\text{C5})$$

while in the opposite limit ($b \ll \Delta b^x$), we get

$$t_1 \sim \frac{(\gamma N \Delta b^x)^3}{A^4}, \quad t_2 \sim \frac{\gamma N^{3/2} \Delta b^x}{A^2}, \quad t_3 \sim \frac{N(\gamma \Delta b^x)^{1/3}}{A^{4/3}}. \quad (\text{C6})$$

Material	A (MHz)	γ (MHz/T)	N	B_{\min}^M
GaAs	1.3×10^5	60	4.4×10^6	50 mT
Si	320	53	10^4	0.3 mT
Si:P	320	53	250	60 mT

TABLE I: Minimum longitudinal fields B_{\min}^M below which the Magnus expansion can fail to describe narrowed-state FID.

Small longitudinal field limit ($b \ll \Delta b^x$)			
GaAs	$\Delta B^x = 25$ mT	$\Delta B^x = 100$ mT	$\Delta B^x = 200$ mT
t_{crit}	800 ns	1.2 μs	1.5 μs
Si	$\Delta B^x = 20$ mT	$\Delta B^x = 80$ mT	$\Delta B^x = 400$ mT
t_{crit}	4.5 μs	7.5 μs	13 μs
Large longitudinal field limit ($b \gg \Delta b^x$)			
GaAs	$B = 200$ mT	$B = 295$ mT	$B = 695$ mT
t_{crit}	1.5 μs	3 μs	12 μs
Si:P	$B = 10$ mT	$B = 20$ mT	$B = 100$ mT
t_{crit}	0.5 μs	1.5 μs	20 μs

TABLE II: Timescales t_{crit} below which the Magnus expansion is valid, according to Eqs. (C5) and (C6). Unless specified otherwise in the table, parameters for lateral dots are those taken from Figs. 3 and 4, considering double dots.

If $t_{\text{crit}} = \min\{t_i\}$ is shorter than the predicted dephasing time from the leading-order Magnus expansion, we conclude that the approximation is not valid. This approach is especially convenient to fix a validity condition for narrowed-state free-induction decay, since there is no motional averaging in that regime. For $b \gg \Delta b^x$, comparing T_{2e}^∇ from Eq. (22) to the above three timescales sets three criteria on Δb^x , of which the most stringent is

$$\lambda \equiv \frac{\Delta b^x}{b} < \frac{N^{5/6} \gamma b}{A}. \quad (\text{C7})$$

Considering a worst-case scenario with $\lambda \sim 1$, this criterion becomes $b > A/\gamma N^{5/6} = b_{\min}^M$. Such minimum values $B_{\min}^M = b_{\min}^M / g^* \mu_B$ in the three main classes of devices studied here are displayed in Table I. These numbers allow us to conclude that keeping only the leading order in the Magnus expansion is a good approximation in all the free-induction cases considered here.

For Hahn-echo decay, it is less convenient to fix a boundary on parameters, because motional averaging can keep coherence finite for long times. Thus, we directly study the timescales beyond which the Magnus expansion can fail. These timescales are calculated in dots and donor impurities for the various parameter regimes studied in this paper and are presented in Table II. In situations where decay occurs in a finite time T_{2e}^∇ , that decay time is always shorter than t_{crit} , except in single donors. In situations where motional averaging is predicted, no discrepancy between the Magnus expansion and the exact numerical solution is seen. We emphasize that the analysis done here only gives us critical times

t_{crit} below which the leading-order term in the Magnus expansion is sure to dominate, but does not determine where the subleading-order term becomes dominant. In other words, we believe these estimates give a definite range of applicability, but the approximations introduced may well be valid outside of that range.

Appendix D: Validity of the Gaussian approximation

In this Appendix, we find a simple criterion which, if respected, justifies the Gaussian approximation. In Section III B, we found that the coherence factor is related to $\langle e^{i\delta\hat{X}(\tau)} \rangle$, which can be expanded in its Taylor series

$$\langle e^{i\delta\hat{X}} \rangle = \sum_n \frac{i^n}{n!} \sum_{k_1 \dots k_n} \sum_{l_1 \dots l_n} h_{k_1}^{l_1} \dots h_{k_n}^{l_n} \langle \delta\hat{I}_{k_1}^{l_1} \dots \delta\hat{I}_{k_n}^{l_n} \rangle. \quad (\text{D1})$$

Since we have taken a bath for which nuclei are uncorrelated, we have $\langle \delta\hat{I}_{k_1}^{l_1} \delta\hat{I}_{k_2}^{l_2} \rangle = \langle \delta\hat{I}_{k_1}^{l_1} \rangle \langle \delta\hat{I}_{k_2}^{l_2} \rangle = 0 \forall k_1 \neq k_2$, by definition of $\delta\hat{I}_k$. To simplify the notation, in this Appendix, we define $\delta\hat{X} \equiv \delta_\chi \hat{X}$ and $\delta\hat{\mathbf{I}}_k \equiv \delta_\chi \hat{\mathbf{I}}_k$ and drop the χ index in expectation values. Thus, we have

$$\langle e^{i\delta\hat{X}(\tau)} \rangle \simeq \sum_n \frac{i^{2n}}{(2n)!} a_n \sum_{kl} \prod_{q=1}^n h_{k_q}^{l_q} h_{k'_q}^{l'_q} \langle \delta\hat{I}_{k_q}^{l_q} \delta\hat{I}_{k'_q}^{l'_q} \rangle, \quad (\text{D2})$$

with $a_n = (2n)!/2^n n!$ the number of ways to group $2n$ terms into n pairs. In the above, we have dropped all moments of order greater than two, which lead to non-Gaussian contributions. The above sums can then be reorganized to yield

$$\langle e^{i\delta\hat{X}(\tau)} \rangle \simeq \exp \left[-\frac{1}{2} \sum_{kl} h_k^l(\tau) h_{k'}^{l'}(\tau) \langle \delta\hat{I}_k^l \delta\hat{I}_{k'}^{l'} \rangle \right], \quad (\text{D3})$$

which is the Gaussian approximation used in Section III B and throughout the paper.

To justify the omission of the moments of order larger than two, we invoke the large number N of nuclei. Indeed, there are roughly N times less elements in a sum of the form $\sum_{k_1 \dots k_n}$ over moments of order 3 than in a similar sum over moments of order 2. Furthermore, in both thermal and narrowed states, we find that moments of odd order vanish. Thus, in order to find the conditions under which the Gaussian approximation is justified, we estimate the importance of the sum over fourth-order moments. Considering only products of these fourth-order moments, we find that the non-Gaussian contributions are of the order of

$$C_4(\tau) \sim \sum_n \frac{i^{4n} b_n}{(4n)!} \sum_{q=1}^n \prod h_{k_q}^{l_q} h_{k'_q}^{l'_q} h_{k''_q}^{l''_q} h_{k'''_q}^{l'''_q} \langle \delta\hat{I}_{k_q}^{l_q} \delta\hat{I}_{k'_q}^{l'_q} \delta\hat{I}_{k''_q}^{l''_q} \delta\hat{I}_{k'''_q}^{l'''_q} \rangle, \quad (\text{D4})$$

with $b_n = (4n)!/24^n n!$ the number of ways to group $4n$ terms into strings of four. For a nuclear-spin bath ini-

tially in a narrowed state, this leads us to

$$C_4(t) \sim \exp \left\{ \frac{1}{24} \sum_k [(h_k^x(t))^4 + (h_k^y(t))^4] \right\}. \quad (\text{D5})$$

For $b \gg \Delta b^x$, this becomes

$$C_4(t) \sim \exp \left[\sum_k \left(\frac{A_k b_k^x t}{b} \right)^4 \right]. \quad (\text{D6})$$

Thus, non-Gaussian contributions grow like $\exp[(t/\tau_4)^4]$, with $1/\tau_4 \sim A\Delta b^x/N^{3/4}b$, while Gaussian contributions led to $\exp[-(t/T_2^\nabla)^2]$ decay. Comparing $1/\tau_4$ and $1/T_2^\nabla \sim A\Delta b^x/N^{1/2}b$, we find that $\tau_4/T_2^\nabla \sim N^{1/4}$, and thus that non-Gaussian contributions only decay as a weak power law as N is increased.

In the case of Hahn echo, we rather find

$$C_4(2t) \sim \exp \left\{ \sum_{k\alpha} [h_k^\alpha(t)]^4 \right\}. \quad (\text{D7})$$

Taking $b \ll \Delta b^x$, if the short-time expansion is valid, we can expand the sines and cosines in the fields $h_k^\alpha(t)$ to leading order in t . We obtain $C_4(2t) \sim \exp[(t/\tau_8)^8]$, and we find $\tau_8/T_2^\nabla \sim N^{1/8}$. Another relevant limit is when $b \gg \Delta b^x$, useful to describe motional averaging. We can then replace $\omega_k \rightarrow b$ and the argument of the exponential becomes an oscillating function with amplitude $\sim (A_k b_k^x)^4/b^8$. Requiring this term to be smaller than the equivalent amplitude for the Gaussian term, discussed in Section IV B, we find that the following criterion must be met

$$\lambda = \frac{\Delta b^x}{b} < \frac{\sqrt{N}\gamma b}{A}. \quad (\text{D8})$$

This criterion is easily satisfied in all materials studied here, even in single P donor impurities in Si, in accordance with the fact that the Gaussian approximation does not fail to predict motional averaging in that material [see Fig. 5(b)].

Appendix E: Σ_s^2 for relevant geometries

As shown in Section IV, both the free-induction and Hahn-echo dephasing times can be linked to the sum $\Sigma_s^2 = \sum_{k_s} (A_{k_s} b_{k_s}^x)^2$. In this section, we calculate Σ_s^2 for various geometries. To simplify the notation, we will drop the species index s .

In all cases, we assume a transverse magnetic field of the form $B^x(\mathbf{r}) = \beta z$, with β a constant, such that

$$b_k^x = z_k \partial_z b^x|_{z=0} = \frac{r_k \cos \theta_k}{r_0} \delta b^x = \sqrt{\frac{k}{N}} \delta b^x \cos \theta_k, \quad (\text{E1})$$

where θ_k is the polar angle locating nucleus k and nuclei are labeled with increasing r_k , as in Appendix A. We have also defined $\delta b^x \equiv r_0 \partial_z b^x|_{z=0}$.

Using Eqs. (A1) and (E1), we calculate Σ^2 for a single dot assuming an isotropic distribution of nuclear spins, with N large enough to convert the sum into an integral. We obtain

$$\Sigma^2 = \frac{1}{d} \frac{(A\delta b^x)^2}{N^{\frac{d}{2}} 2^{\frac{2+d}{q}} \Gamma^2\left(\frac{d}{q}\right)} \Gamma\left(\frac{2+d}{q}\right). \quad (\text{E2})$$

In the specific case of $d = q = 2$, this yields $\Sigma^2 = (A\delta b^x)^2/8N$.

For double dots with $d = q = 2$, we rather use Eqs. (A4) and (B3) for A_k . In the case of a single electron with a symmetric (+) or antisymmetric (−) delocalized

wavefunction $\psi_{\pm}(\mathbf{r})$ as in Appendix A, we get

$$\Sigma^2 = \left(\frac{A\delta b^x}{e^{\eta^2} \pm 1}\right)^2 \frac{3 \pm 4e^{\eta^2/2}(1 + \eta^2) + e^{2\eta^2}(1 + 4\eta^2)}{16N}. \quad (\text{E3})$$

Different wavefunctions lead to different values of Σ^2 because we have taken into account the overlap between the orbitals. For a singlet-triplet qubit, we rather have

$$\Sigma^2 = (A\delta b^x)^2 \frac{1 + 4\eta^2 - e^{-2\eta^2}}{4N}. \quad (\text{E4})$$

-
- ¹ F. H. L. Koppens, K. C. Nowack, and L. M. K. Vander-sypen, *Phys. Rev. Lett.* **100**, 236802 (2008), URL <http://link.aps.org/doi/10.1103/PhysRevLett.100.236802>.
- ² H. Bluhm, S. Foletti, I. Neder, M. Rudner, D. Mahalu, V. Umansky, and A. Yacoby, *Nature Physics* **7**, 109 (2010).
- ³ A. V. Khaetskii, D. Loss, and L. Glazman, *Phys. Rev. Lett.* **88**, 186802 (2002), URL <http://link.aps.org/doi/10.1103/PhysRevLett.88.186802>.
- ⁴ B. Maune, M. Borselli, B. Huang, T. Ladd, P. Deelman, K. Holabird, A. Kiselev, I. Alvarado-Rodriguez, R. Ross, A. Schmitz, et al., *Nature* **481**, 344 (2012).
- ⁵ W. A. Coish, J. Fischer, and D. Loss, *Phys. Rev. B* **77**, 125329 (2008), URL <http://link.aps.org/doi/10.1103/PhysRevB.77.125329>.
- ⁶ W. A. Coish, J. Fischer, and D. Loss, *Phys. Rev. B* **81**, 165315 (2010), URL <http://link.aps.org/doi/10.1103/PhysRevB.81.165315>.
- ⁷ W. M. Witzel and S. Das Sarma, *Phys. Rev. B* **74**, 035322 (2006), URL <http://link.aps.org/doi/10.1103/PhysRevB.74.035322>.
- ⁸ L. Cywiński, W. M. Witzel, and S. Das Sarma, *Phys. Rev. Lett.* **102**, 057601 (2009), URL <http://link.aps.org/doi/10.1103/PhysRevLett.102.057601>.
- ⁹ L. Cywiński, W. M. Witzel, and S. Das Sarma, *Phys. Rev. B* **79**, 245314 (2009), URL <http://link.aps.org/doi/10.1103/PhysRevB.79.245314>.
- ¹⁰ L. Cywiński, V. V. Dobrovitski, and S. Das Sarma, *Phys. Rev. B* **82**, 035315 (2010), URL <http://link.aps.org/doi/10.1103/PhysRevB.82.035315>.
- ¹¹ E. Barnes, L. Cywiński, and S. Das Sarma, *Phys. Rev. Lett.* **109**, 140403 (2012), URL <http://link.aps.org/doi/10.1103/PhysRevLett.109.140403>.
- ¹² J. R. Klauder and P. W. Anderson, *Phys. Rev.* **125**, 912 (1962), URL <http://link.aps.org/doi/10.1103/PhysRev.125.912>.
- ¹³ W. M. Witzel, R. de Sousa, and S. Das Sarma, *Phys. Rev. B* **72**, 161306 (2005), URL <http://link.aps.org/doi/10.1103/PhysRevB.72.161306>.
- ¹⁴ W. Yao, R. B. Liu, and L. J. Sham, *Phys. Rev. B* **74**, 195301 (2006).
- ¹⁵ A. Morello, J. Pla, F. Zwanenburg, K. Chan, K. Tan, H. Huebl, M. Möttönen, C. Nugroho, C. Yang, J. van Donkelaar, et al., *Nature* **467**, 687 (2010).
- ¹⁶ J. Pla, K. Tan, J. Dehollain, W. Lim, J. Morton, D. Jamieson, A. Dzurak, and A. Morello, *Nature* **489**, 541 (2012).
- ¹⁷ M. Pioro-Ladrière, T. Obata, Y. Tokura, Y. Shin, T. Kubo, K. Yoshida, T. Taniyama, and S. Tarucha, *Nature Physics* **4**, 776 (2008).
- ¹⁸ T. Obata, M. Pioro-Ladrière, Y. Tokura, Y.-S. Shin, T. Kubo, K. Yoshida, T. Taniyama, and S. Tarucha, *Phys. Rev. B* **81**, 085317 (2010), URL <http://link.aps.org/doi/10.1103/PhysRevB.81.085317>.
- ¹⁹ X. Hu, Y.-x. Liu, and F. Nori, *Phys. Rev. B* **86**, 035314 (2012), URL <http://link.aps.org/doi/10.1103/PhysRevB.86.035314>.
- ²⁰ T. Frey, P. J. Leek, M. Beck, A. Blais, T. Ihn, K. Ensslin, and A. Wallraff, *Phys. Rev. Lett.* **108**, 046807 (2012), URL <http://link.aps.org/doi/10.1103/PhysRevLett.108.046807>.
- ²¹ K. D. Petersson, L. W. McFaul, M. D. Schroer, M. Jung, J. M. Taylor, A. A. Houck, and J. R. Petta, *Nature* **490**, 380 (2012).
- ²² M. Trif, V. N. Golovach, and D. Loss, *Phys. Rev. B* **77**, 045434 (2008), URL <http://link.aps.org/doi/10.1103/PhysRevB.77.045434>.
- ²³ W. A. Coish and D. Loss, *Phys. Rev. B* **70**, 195340 (2004), URL <http://link.aps.org/doi/10.1103/PhysRevB.70.195340>.
- ²⁴ D. Klauser, W. A. Coish, and D. Loss, *Phys. Rev. B* **73**, 205302 (2006), URL <http://link.aps.org/doi/10.1103/PhysRevB.73.205302>.
- ²⁵ D. Stepanenko, G. Burkard, G. Giedke, and A. Imamoglu, *Phys. Rev. Lett.* **96**, 136401 (2006).
- ²⁶ G. Giedke, J. M. Taylor, D. D'Alessandro, M. D. Lukin, and A. Imamoglu, *Phys. Rev. A* **74**, 032316 (2006).
- ²⁷ H. Bluhm, S. Foletti, D. Mahalu, V. Umansky, and A. Yacoby, *Phys. Rev. Lett.* **105**, 216803 (2010), URL <http://link.aps.org/doi/10.1103/PhysRevLett.105.216803>.
- ²⁸ J. Fischer, W. A. Coish, D. V. Bulaev, and D. Loss, *Phys. Rev. B* **78**, 155329 (2008), URL <http://link.aps.org/doi/10.1103/PhysRevB.78.155329>.
- ²⁹ B. Eble, C. Testelin, P. Desfonds, F. Bernardot, A. Balocchi, T. Amand, A. Miard, A. Lemaître, X. Marie, and M. Chamarro, *Phys. Rev. Lett.* **102**, 146601 (2009).
- ³⁰ D. Brunner, B. D. Gerardot, P. A. Dalgarno, G. Wüst, K. Karrai, N. G. Stoltz, P. M. Petroff, and R. J. Warburton, *Science* **325**, 70 (2009).
- ³¹ K. De Greve, P. L. McMahon, D. Press, T. D. Ladd, D. Bisping, C. Schneider, M. Kamp, L. Worschech,

- S. Höfling, A. Forchel, et al., Nature Physics **7**, 872 (2011).
- ³² X. J. Wang, S. Chesi, and W. A. Coish, Phys. Rev. Lett. **109**, 237601 (2012), URL <http://link.aps.org/doi/10.1103/PhysRevLett.109.237601>.
- ³³ S. Nadj-Perge, S. Frolov, E. Bakkers, and L. Kouwenhoven, Nature **468**, 1084 (2010).
- ³⁴ E. Fermi, Zeitschrift für Physik **60**, 320 (1930), ISSN 0044-3328, URL <http://dx.doi.org/10.1007/BF01339933>.
- ³⁵ W. M. Witzel, X. Hu, and S. Das Sarma, Phys. Rev. B **76**, 035212 (2007), URL <http://link.aps.org/doi/10.1103/PhysRevB.76.035212>.
- ³⁶ S. Saikin and L. Fedichkin, Phys. Rev. B **67**, 161302 (2003), URL <http://link.aps.org/doi/10.1103/PhysRevB.67.161302>.
- ³⁷ D. P. Burum, Phys. Rev. B **24**, 3684 (1981).
- ³⁸ M. M. Maricq, Phys. Rev. B **25**, 6622 (1982), URL <http://link.aps.org/doi/10.1103/PhysRevB.25.6622>.
- ³⁹ J.-T. Hung, L. Cywiński, X. Hu, and S. Das Sarma, ArXiv e-prints (2013), 1304.6711, URL <http://adsabs.harvard.edu/abs/2013arXiv1304.6711H>.
- ⁴⁰ R. Brunner, Y.-S. Shin, T. Obata, M. Pioro-Ladrière, T. Kubo, K. Yoshida, T. Taniyama, Y. Tokura, and S. Tarucha, Phys. Rev. Lett. **107**, 146801 (2011), URL <http://link.aps.org/doi/10.1103/PhysRevLett.107.146801>.
- ⁴¹ W. A. Coish and J. Baugh, Physica Status Solidi (b) **246**, 2203 (2009), ISSN 1521-3951, URL <http://dx.doi.org/10.1002/pssb.200945229>.
- ⁴² L. V. C. Assali, H. M. Petrilli, R. B. Capaz, B. Koiller, X. Hu, and S. Das Sarma, Phys. Rev. B **83**, 165301 (2011), URL <http://link.aps.org/doi/10.1103/PhysRevB.83.165301>.
- ⁴³ J. Petta, A. Johnson, J. Taylor, E. Laird, A. Yacoby, M. Lukin, C. Marcus, M. Hanson, and A. Gossard, Science **309**, 2180 (2005).
- ⁴⁴ J. Schliemann, A. Khaetskii, and D. Loss, Journal of Physics: Condensed Matter **15**, R1809 (2003).
- ⁴⁵ W. M. Witzel, M. S. Carroll, L. Cywiński, and S. Das Sarma, Phys. Rev. B **86**, 035452 (2012), URL <http://link.aps.org/doi/10.1103/PhysRevB.86.035452>.
- ⁴⁶ A. M. Tyryshkin, S. A. Lyon, A. V. Astashkin, and A. M. Raitsimring, Phys. Rev. B **68**, 193207 (2003), URL <http://link.aps.org/doi/10.1103/PhysRevB.68.193207>.
- ⁴⁷ E. Abe, A. M. Tyryshkin, S. Tojo, J. J. L. Morton, W. M. Witzel, A. Fujimoto, J. W. Ager, E. E. Haller, J. Isoya, S. A. Lyon, et al., Phys. Rev. B **82**, 121201 (2010), URL <http://link.aps.org/doi/10.1103/PhysRevB.82.121201>.
- ⁴⁸ B. Kane, Nature **393**, 133 (1998).
- ⁴⁹ W. A. Coish and D. Loss, Phys. Rev. B **72**, 125337 (2005), URL <http://link.aps.org/doi/10.1103/PhysRevB.72.125337>.
- ⁵⁰ D. Paget, G. Lampel, B. Sapoval, and V. Safarov, Phys. Rev. B **15**, 5780 (1977).
- ⁵¹ Anisotropic hyperfine interactions of the form $\sum_k (A_k^x \hat{I}_k^x + A_k^z \hat{I}_k^z) \hat{S}_z$ can easily be accounted for within our theoretical framework if each nuclear spin is rotated by an angle $\theta_k = \arctan(A_k^x/A_k^z)$ around the y -axis by applying the operators $\hat{R}_k^y(\theta) = \exp(-i\theta_k \hat{I}_k^y)$. We retrieve a Hamiltonian that has the exact same form as Eq. (1), but with modified coupling constants $A_k \rightarrow \sqrt{(A_k^x)^2 + (A_k^z)^2}$, gyromagnetic ratios $\gamma_k \rightarrow \gamma_k (b_k^x A_k^x + b_k^z A_k^z) / b_k A_k'$, and transverse fields $b_k^x \rightarrow b_k (b_k^x A_k^z - b_k^z A_k^x) / (b_k A_k^z + b_k^x A_k^x)$. However, this approach will not reproduce exactly the same Hamiltonian in the presence of terms proportional to $\sum_k A_k \hat{I}_k^y \hat{S}_z$, but should lead to similar qualitative behavior, especially if the anisotropic hyperfine coupling terms are weak.
- ⁵² Deviations from the predictions of the approximation $(m_k^j)^2 \rightarrow \sum_m p(m) m^2$ were numerically checked to be negligible even for systems as small as single phosphorus donors in silicon, where $N \simeq 250$. This is not surprising, since this approximation works when there is a large number of nuclear-spin configurations that lead to the same average polarization in a small region of space. That number of configurations, and thus the quality of the approximation, grows exponentially with N , in contrast with the Gaussian approximation, which improves as a power law in N .
- ⁵³ In the absence of measured narrowed-state decay in Si, we compare the FID decay time T_2^∇ to the $1/e$ -decay time $2T_{2,e}$ for Hahn echo accounting for the full 2τ duration between initialization and echo.